Research Highlights

[FY2025]

Japan International Research Center for Agricultural Sciences

Meeting global challenges through research and technology development

JIRCAS
国際農研

A microbial saccharification method for efficient production of high-concentration sugar solutions from rice straw

Rice straw is generated in large quantities across Asia, and open-field burning remains a common disposal method that contributes to air pollution, public health concerns, and transboundary haze problems. Converting rice straw into fermentable sugars provides an environmentally sound alternative and enables the production of biofuels and bio-based chemicals. However, practical application requires high-solids saccharification to obtain concentrated sugar solutions that improve downstream fermentation and purification efficiency. Conventional saccharification methods rely heavily on externally supplied enzymes, creating cost and supply constraints. This study aimed to develop an enzyme-independent microbial saccharification process capable of stably producing high-concentration sugar solutions under high-solids conditions by optimizing culture operation and incorporating surfactant-based stabilization.

To address instability issues associated with high-solids saccharification, such as poor mixing, non-productive enzyme adsorption, and enzyme inactivation, we examined the effect of adding Tween 20 (a non-ionic surfactant) to a co-culture system comprising *Clostridium thermocellum* and the β-glucosidase-producing strain *Thermobrachium celere* A9. Tween 20 improved the retention of cellulase and β-glucosidase activities, resulting in enhanced and more sustained saccharification performance. In parallel, a semi-continuous operation strategy was developed in which pretreated rice straw was added stepwise during cultivation. Combining Tween 20 with this feeding strategy effectively prevented saccharification stagnation, even at high total solids. Under optimized conditions, a total substrate loading of 250 g L^{-1} yielded 140 g L^{-1} of glucose, corresponding to 70% of the theoretical yield, without the addition of external enzymes. These results demonstrate that both biochemical stabilization and operational design are essential for maintaining saccharification activity at high solids.

This microbial saccharification approach provides a cost-effective and enzyme-independent method for producing concentrated sugar solutions from underutilized biomass such as rice straw. It supports the development of sustainable biomass-to-chemicals pathways in Asia, where large volumes of agricultural residues are generated and environmentally sound disposal options are urgently needed. The semi-continuous feeding concept offers practical insights for scaling up high-solids saccharification, including considerations for substrate handling, mixing, and process control. Further evaluation of alternative low-cost non-ionic surfactants and their impacts on downstream processes will aid in refining industrial applicability. Overall, the system provides a promising foundation for expanding biomass utilization while reducing environmental burdens associated with current disposal practices.

Authors: Nhim, S., Waeonukul, R. [KMUTT], Uke, A., Kosugi, A. [JIRCAS]

Table 1. Effect of Tween 20 (surfactant) addition on microbial saccharification of rice straw

Tween 20 (% v/v)	Accumulated glucose in the medium (gL^{-1})	Glucose yield from the cellulose of rice straw[*1] (%)	Cellulase activity (U/mL)	β-Glucosidase activity (U/mL)
None	78.8 ± 0.2	65.7 ± 0.2	2.5 ± 0.3	3.0 ± 0.2
0.1	82.5 ± 0.3	68.8 ± 0.3	3.3 ± 0.2	4.5± 0.1
0.5	**90.8 ± 0.2**	**75.7 ± 0.2**	**5.2 ± 0.1**	**5.3 ± 0.2**
1.0	80.8 ± 0.5	67.4 ± 0.5	2.8 ± 0.3	4.5 ± 0.3
1.5	54.8 ± 0.5	45.3 ± 0.5	1.3 ± 0.3	1.1 ± 0.1

[*1]Alkali-pretreated rice straw was used (see Nhim et al. (2025) for the pretreatment conditions). Microbial saccharification was carried out using a co-culture of *Clostridium thermocellum* and *Thermobrachium celere* A9, with a rice straw loading of 150 g L^{-1}. Tween 20 was added at the indicated concentrations on a volume/volume basis (% v/v). Values represent the mean ± standard deviation of three independent experiments.

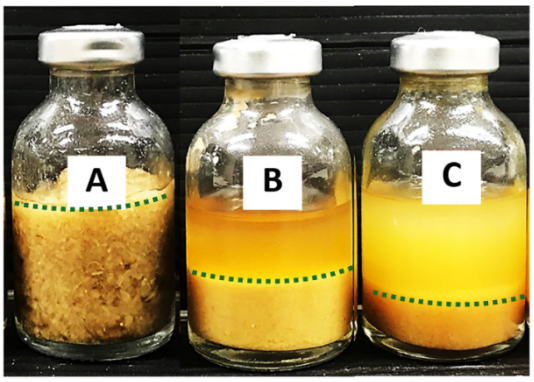

Fig. 1. The effect of Tween 20 (a surfactant) addition on the saccharification of rice straw at a solid loading of 150 g L^{-1} using microbial saccharification

(A) No saccharolytic microorganisms inoculated; (B) Microbial saccharification without Tween 20 addition; (C) Microbial saccharification with 0.5% Tween 20 addition. Lines indicate the remaining amount of substrate during microbial saccharification.

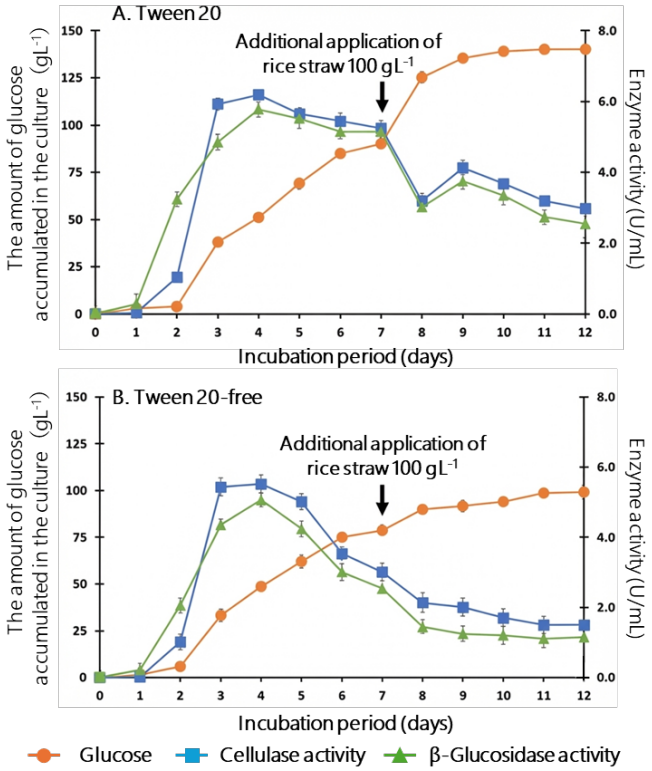

Fig. 2. Semi-continuous microbial saccharification with rice straw

Microbial saccharification was initiated with an initial solid loading of 150 g L^{-1}, followed by the addition of pretreated rice straw at a concentration of 100 g L^{-1}. (A) With Tween 20; (B) Without Tween 20. Arrows indicate the time points at which the rice straw was added. Data are means ± SD (n = 3).

Reference: Nhim et al. (2025) *Frontiers in Microbiology* 15, 1519060. © Authors 2025
The table and figures are reprinted/modified from Nhim et al. (2025) under the terms of the CC-BY 4.0 license.
https://creativecommons.org/licenses/by/4.0/deed.en

Regional environmental adaptability of teak genetic resources based on genomic analysis and utilization strategies under climate change

As global temperatures rise and rainfall patterns shift, forest ecosystems—and specifically long-lived trees—face a critical challenge, as they cannot simply relocate to more favorable climates. For a high-economic-value species like teak (*Tectona grandis*), which is used for high-end furniture production across approximately 65 countries, building resilience into plantation strategies is no longer optional but essential. In Indonesia, teak has been a staple of the timber industry for generations, yet there is an unresolved question regarding its heritage; while it was once thought to be of Indian origin, a recent study reveals that these trees are more genetically related to Indochinese populations. This research seeks to bridge that gap by using genomic data to decode the relationship between genetic diversity and climate adaptability, with the goal of future-proofing Indonesian plantations for long-term, sustainable wood production.

The study's genomic analysis reveals that populations in India harbor significantly higher genetic variation than those in other regions, with the Malabar group in southern India showing the most distinct genetic differentiation. A key discovery from the association analysis between genetic markers and climate factors is that temperature—specifically the mean temperature during the rainy season—is a far more significant evolutionary driver for teak than rainfall. These results point to a high number of genomic regions linked to thermal shifts, suggesting that the Malabar and North Indian populations possess a natural resilience to heat. This is particularly relevant for the future of Indonesian forestry, as climate models predict that the future environment of Java will resemble that of the Malabar region, making those southern Indian genetic resources ideal candidates for climate adaptation.

These findings provide a robust scientific framework for selecting tree provenances and managing genetic resources in a warming world. By strategically introducing genetic variants from the Malabar population through seed migration or targeted crossbreeding, forestry managers can effectively "upgrade" Indonesian plantations to withstand predicted climate shifts. However, the introduction of these genetic lineages requires a cautious, phased approach. It is vital to conduct long-term evaluations to monitor potential hybridization with local populations and to ensure that genetic diversity is maintained without compromising growth characteristics or resistance to local pests and diseases.

Authors: Tani, N. [JIRCAS], Onuma, Y., Tsumura Y. [Univ. of Tsukuba],
Prasetyo, E., Widiyatno, Indrioko, S., Na'iem, M. [UGM]

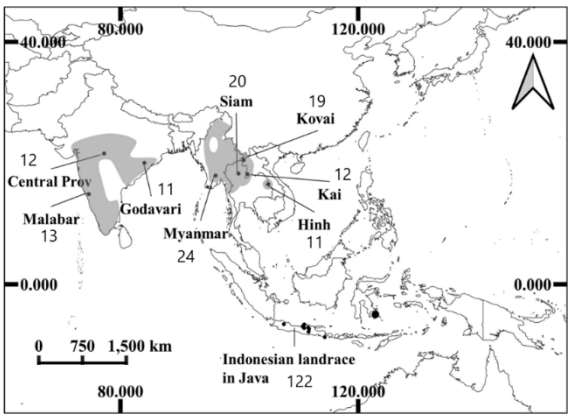

Fig. 1. Natural distribution of teak and locations of populations sampled in Indonesian international provenance trials

Shaded areas represent the natural range; black circles indicate the origin of sampled individuals; numbers indicate the number of individuals used in genomic analysis.

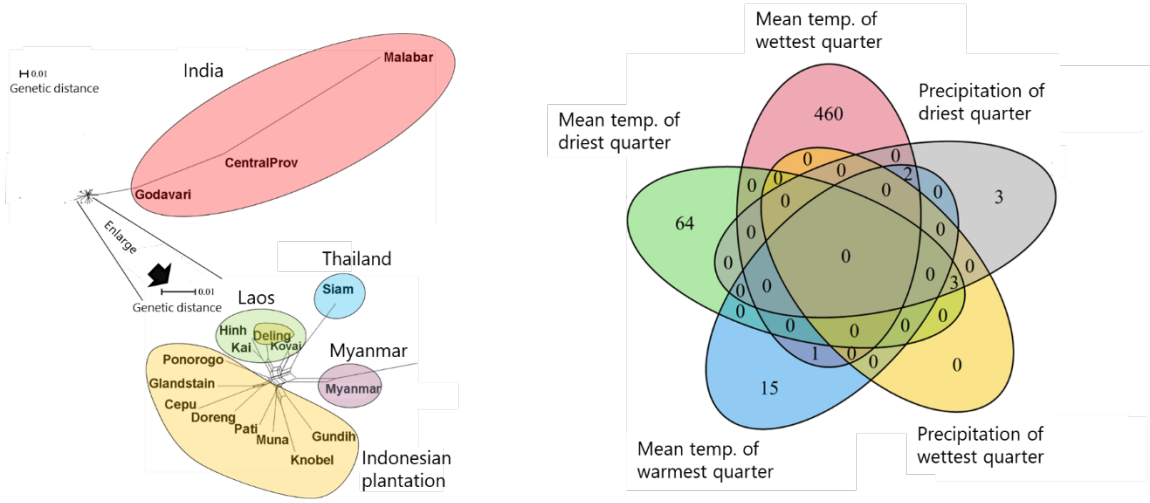

Fig. 2. Genetic differences among teak populations and the number of loci significantly associated with bioclimatic variables in natural populations

(A) The dendrogram shows significant genetic differences between the three Indian populations and others. (B) 460 SNPs are associated with rainy season mean temperature, compared to 64 for the dry season.

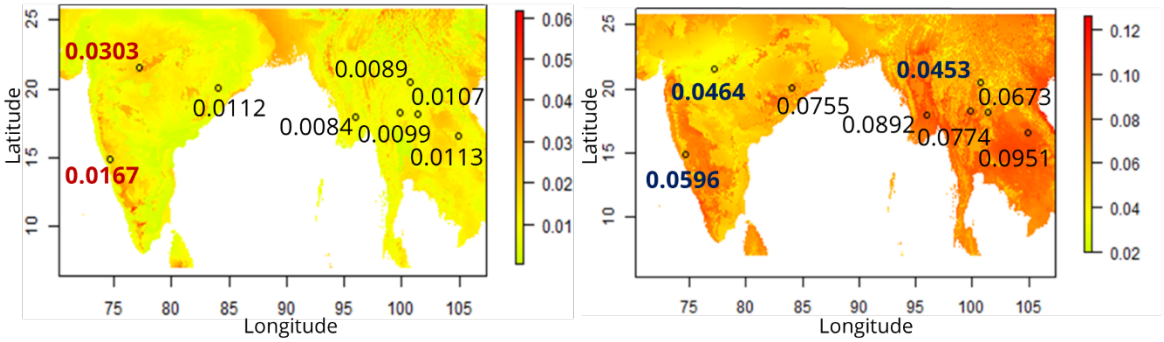

Fig. 3. Levels of regional environmental adaptation and resilience to future climate change

(A) Larger numbers indicate stronger genetic adaptation to the local environment (highest in two Indian populations). (B) Simulations under the SSP5-8.5 scenario show that smaller values indicate stronger resilience. Note: Laos shows a small value, but this may be "pseudo-resilience" due to low temperature change in high-altitude areas.

Reference: Onuma et al. (2025) *Forest Science and Technology* 21: 252–272. © Authors 2025
The figures are reprinted/modified from Onuma et al. (2025) under the terms of the CC-BY 4.0 license.
https://creativecommons.org/licenses/by/4.0/deed.en

Leaf nitrogen concentration indicates the growth rate of *Falcataria falcata*, a major fast-growing tree in Southeast Asia

Falcataria falcata, a leguminous tree native to Indonesia, the Solomon Islands, and Papua New Guinea, is among the fastest-growing tree species in the world. Owing to its moderate wood strength and good workability, its timber is in high demand for wood products such as laminated lumber and plywood. However, growth rates vary greatly among individuals even within the same plantation. To improve wood productivity, it is essential to select fast-growing individuals and achieve more uniform growth in plantations. Identifying simple traits associated with growth rate would help shorten the time required for selecting superior trees. Leaf traits such as photosynthetic rate and specific leaf area (SLA) often correlate with growth rate, potentially serving as useful indicators. For *F. falcata*, however, differences in growth rate and leaf traits among genetically different populations remain unclear. In this study, we examined the relationships between growth rate, photosynthetic rate, and leaf traits among genetically different populations originating from Indonesia and the Solomon Islands.

Seeds of *F. falcata* collected from nine locations in Indonesia and the Solomon Islands (Fig. 1A) were grown under common environmental conditions (Fig. 1B). Relative growth rate (RGR)* over three weeks (Fig. 2), maximum leaf photosynthetic rate**, and leaf nitrogen concentration varied greatly among populations, whereas no significant differences were observed in SLA. The population-mean of leaf nitrogen concentration was positively associated with that of maximum leaf photosynthetic rate (Fig. 3) and RGR (Fig. 4).

These results suggest that leaf nitrogen concentration can be used as an indicator of growth performance and can accelerate the selection of fast-growing individuals. We also suggest that growth rate and photosynthetic traits in *F. falcata* have a genetic basis. These traits can therefore be utilized in breeding programs to develop varieties with superior growth performance and physiological characteristics. Conducting similar assessments in plantations and in mature trees will further strengthen the applicability of these findings.

*Relative growth rate (RGR): growth rate per unit biomass, where higher values indicate more efficient growth

**Maximum leaf photosynthetic rate: the maximum rate of leaf photosynthesis measured under non-limiting conditions of light, water, and temperature

Authors: Kawai, K., Kenzo, T., Tani, N. [JIRCAS],
Faridah, E., Figyantika, A., Romadini, N. P., Sawitri, Prehaten, D., Widiyatno, Na'iem, M. [UGM],
Tsumura, Y. [Univ. of Tsukuba]

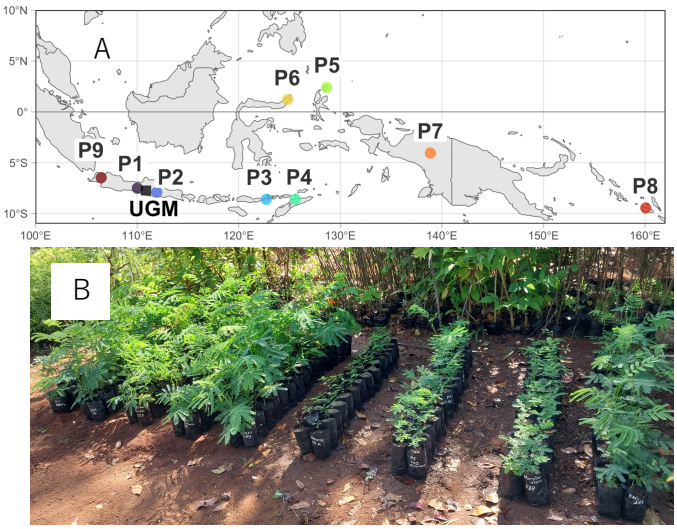

Fig. 1. Locations of seed collection of *Falcataria falcata* and Universitas Gadjah Mada (UGM) (A), and seedlings of *F. falcata* (B)

(A) Circles indicate the locations where *Falcataria falcata* seeds were collected, and the square indicates the location of Universitas Gadjah Mada (UGM). The labels represent populations. Seeds were collected from three plantations on Java Island (P1, P2, and P9) and from natural forests at all other sites. (B) *F. falcata* seedlings grown in the UGM's experimental forest.

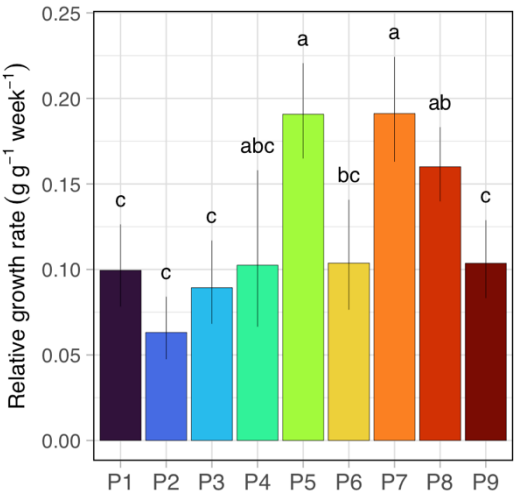

Fig. 2. Relative growth rate (RGR) of *F. falcata* across populations

Different letters indicate significant differences among populations based on Tukey's HSD test ($p < 0.05$). Error bars represent 95% confidence intervals (n = 29–30). Bar colors correspond to the populations shown in Fig. 1.

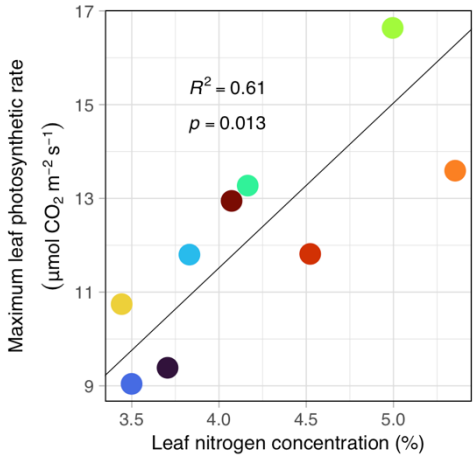

Fig. 3. Relationship between leaf nitrogen concentration and maximum leaf photosynthetic rate

Point colors correspond to the populations shown in Fig. 1, and the solid line represents the fitted linear regression. Each point represents the mean of five individuals.

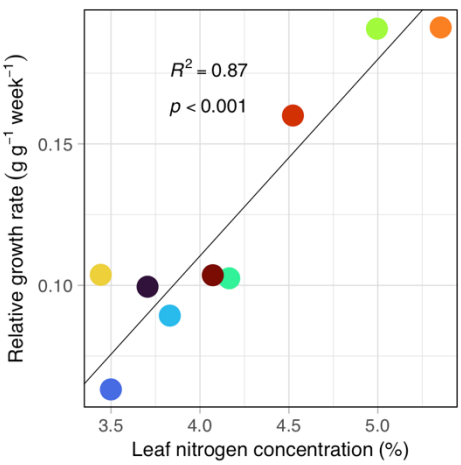

Fig. 4. Relationship between leaf nitrogen concentration and RGR

Point colors correspond to the populations shown in Fig. 1, and the solid line represents the fitted linear regression. For each point, leaf nitrogen concentration represents the mean of five individuals, and RGR represents the mean of 29–30 individuals.

Reference: Faridah et al. (2025) *Trees–Structure and Function* 39: 78. © Springer 2025
The figures are reprinted/modified from Faridah et al. (2025) with permission.

Visualizing the effect of production and consumer efforts on nitrogen load reduction using the food nitrogen footprint concept

Issues related to reactive nitrogen (Nr) continue to increase and have exceeded planetary boundaries. Both production- and consumer-level efforts can mitigate Nr loads and inputs. However, only independent evaluations of these efforts have been performed thus far, and the lack of comprehensive evaluations has hindered further reductions in Nr loads and inputs. Therefore, in this study, we applied the food nitrogen footprint to Ishigaki Island, Japan, and evaluated both direct (on-island) and indirect (overseas-related, i.e., imported food/feed production) Nr loads and inputs within the food system.

We calculated the food nitrogen footprint using official statistical data from Ishigaki City for 2022. For data unavailable at the city scale, we applied statistical data on food/feed production from the prefectural and national scales and data from previous studies. The amount of imported food Nr was estimated by compensating for the deficit in the food on the island using the food demand for Japan in 2015. The food loss ratio was 11%. We summed the Nr flows for all food items to assess the current Nr situation within the island's food system and to estimate direct and indirect Nr loads and inputs (Fig. 1). To evaluate how production- and consumer-level efforts can mitigate Nr loads and inputs, the following scenarios were developed: (a) shifting diets toward grains and legumes in imported food, (b) halving food loss and using the remainder as concentrate feed, and (c) replacing chemical fertilizers with cattle manure produced on the island. Altering the composition of imported food, reducing food loss by half, and utilizing the remaining portion as feed effectively reduced the indirect Nr load, while using cattle manure reduced the direct Nr load. Implementing these measures in combination reduced the direct and indirect Nr loads by 15% and 31% and the direct and indirect Nr inputs by 20% and 19%, respectively (Fig. 2). Therefore, it is essential to implement consumer and production efforts simultaneously rather than independently to optimize the global nitrogen cycle.

This study allows us to evaluate the effect of production and consumers on the mitigation of Nr loads and inputs. This encourages the establishment of a policy that involves production and consumers and contributes to addressing the SDGs. However, these scenarios do not consider economics. Without showing the actual cost of replacing chemical fertilizers with manure and using food losses as eco-feed, adopting these measures would be difficult, even if they are environmentally beneficial. Exploring scenarios to further reduce Nr loads and inputs, such as applying other agricultural waste to farmland or livestock feed, is essential. These possibilities should be considered in future studies.

Authors: Hamada, K. [JIRCAS], Eguchi, S., Hirano, N., Asada, K. [NARO]

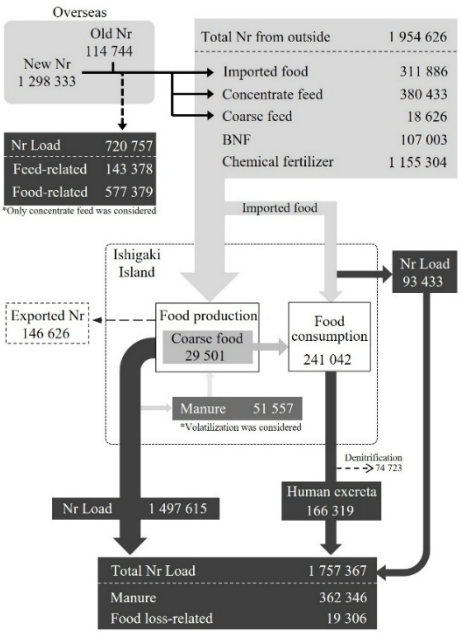

Fig. 1. Current nitrogen flow on Ishigaki Island under present conditions

The unit is kg N. BNF stands for biological nitrogen fixation. New and old Nr indicate chemical fertilizer and manure, respectively.

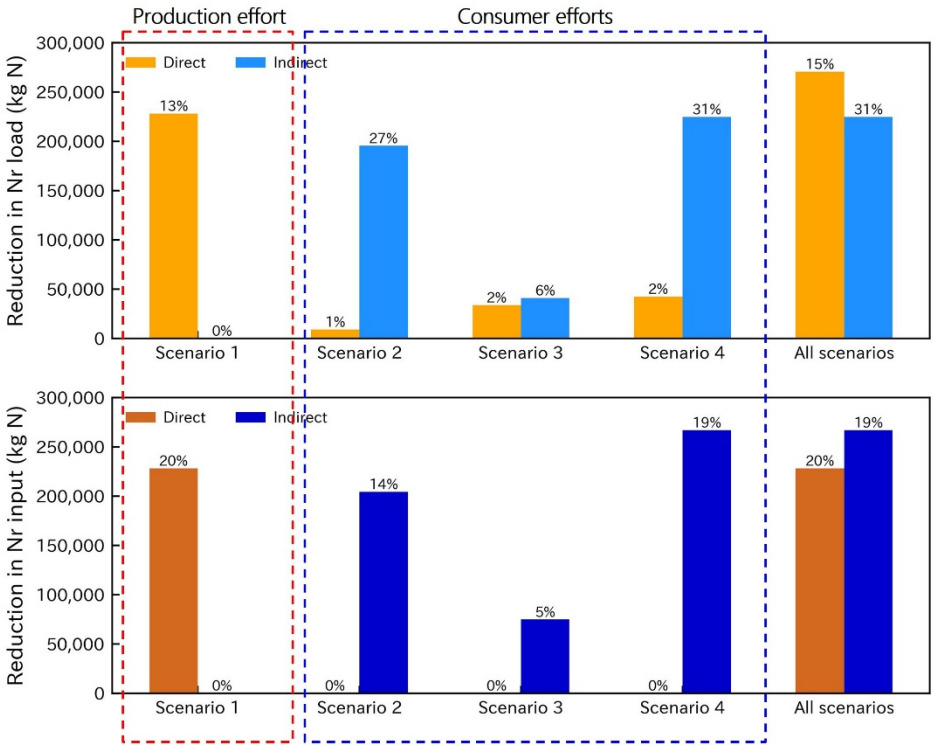

Fig. 2. Reduction in Nr load and input under each scenario

Scenario 1: promotion of manure use; Scenario 2: change in the composition of imported food; Scenario 3: halving food loss and using the remainder as concentrate feed; Scenario 4: combination of Scenarios 2 and 3. "Direct" and "indirect" Nr loads and inputs refer to those on and outside the island, respectively. The direct Nr load contains human excreta. The percentage indicates the reduction rate compared to the present condition.

Reference: Hamada et al. (2025) *Environmental Research Letters* 20: 114017. © Authors 2025
The figures are reprinted/modified from Hamada et al. (2025) under the terms of the CC-BY 4.0 license.
https://creativecommons.org/licenses/by/4.0/deed.en

Technical manual for mitigating soil salinization with preferential shallow sub-surface drainage and sub-surface irrigation

In the Indo-Gangetic Plain (IGP) of northern India, soil salinization is a serious problem due to irrigation using high-salinity groundwater and residual salt accumulation resulting from poor drainage. While improving drainage and adopting water-saving practices are effective countermeasures, the construction of open drainage and sub-surface drainage networks and the introduction of drip or sprinkler systems require significant initial investment and maintenance costs. Shallow sub-surface drainage using a "Cut-soiler" (a tractor attachment developed in Japan), sub-surface irrigation using "water drop tubes," and water-saving gains through improvements in furrow irrigation are relatively inexpensive and easy to implement compared to conventional drainage and water-saving technologies. These promising and sustainable measures, which can be integrated into farming, have been compiled into a technical manual to promote extension activities.

The technical manual, structured into four chapters (Table 1; Fig. 1), is an 80-page, A4-sized booklet that makes extensive use of photographs and illustrations to facilitate understanding. Regarding drainage mitigation, the manual details the structure and construction method of shallow sub-surface drainage with the Cut-soiler, alongside the effects on desalination and pH improvement. It also identifies the optimal construction interval (JIRCAS Research Highlights, FY2022 A11 and FY2024 A10). Furthermore, the manual analyzes seasonal fluctuations in groundwater levels, which share a strong causal relationship with soil salinization, to indicate the optimal construction timing for Cut-soiler drainage. The Cut-soiler's break-even point is clarified (Fig. 2) and a rural adoption system is proposed. As water-saving measures, sub-surface irrigation with water drop tubes, skip furrow irrigation (irrigating every other furrow), and simplified surge flow irrigation (supplying water twice at a one-day interval) (Fig. 3) are introduced. Additionally, the manual identifies soil sodification (an increased proportion of sodium ions) as a primary cause of serious drainage problems and proposes relevant countermeasures.

The technical manual can be used in trainings and/or seminars for widespread dissemination of the effects of shallow sub-surface drainage and sub-surface irrigation. The distribution of the manual is expected to facilitate rapid information sharing among government officials, local organizations, and farmers. While shallow sub-surface drainage and sub-surface irrigation are distinct technologies, if applied together, a greater effect is expected. Although the manual is based on verification within the IGP, it is applicable to similar regions based on an evaluation of irrigation and drainage conditions.

Chaudhari, S.K. [Fertilizer Association of India (FAI)],
Yadav, R.K., Yadav, G., Rai, A.K., Kumar, Su., Kumar, Sa., Narjary, B. [CSSRI],
Onishi, J., Kameoka, T., Matsui, K., Lee, G. [JIRCAS], Kitagawa, I. [NARO]

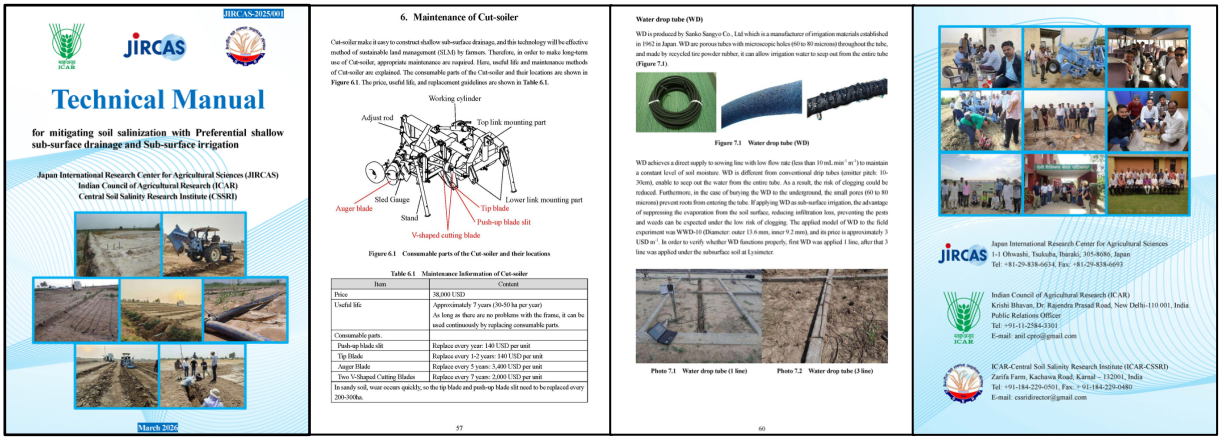

Fig. 1. Technical manual for mitigating soil salinization

Table 1. Contents of technical manual

Chapters	Title	Contents
Chap. 1	Introduction	Status of irrigated agriculture and salinization, Purpose of joint research
Chap. 2	Salinization	Classification of salt-affected soils, Explanation of sodic soils, Salinization in India: Cause and countermeasures
Chap. 3	Cut-soiler	Drainage types, Construction methods using Cut-soilers
Chap. 4	Effect of Cut-soiler	Effects in lysimeter and field trials
Chap. 5	Applicability of Cut-soiler	Economic evaluation of Cut-soiler, Proposed rural adoption system
Chap. 6	Maintenance of Cut-soiler	Service life and maintenance methods for Cut-soilers
Chap. 7	Water-saving	Effects of sub-surface irrigation with water drop tubes, Water-saving skip furrow irrigation and simplified surge flow irrigation

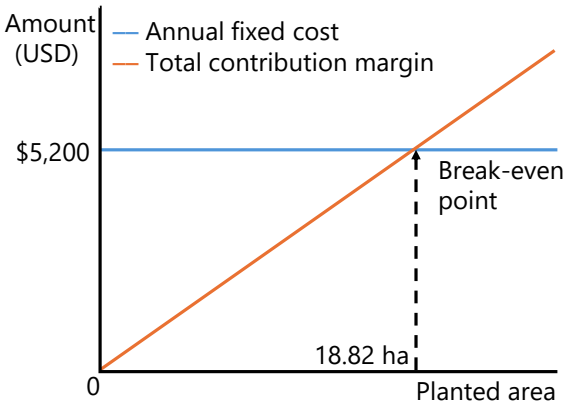

Fig. 2. Break-even point for Cut-soiler

Annual fixed cost: $5,200, calculated by annualizing the purchase cost of approximately $39,000 using a 10% discount rate and a 15-year useful life (Converted at ¥160/USD).

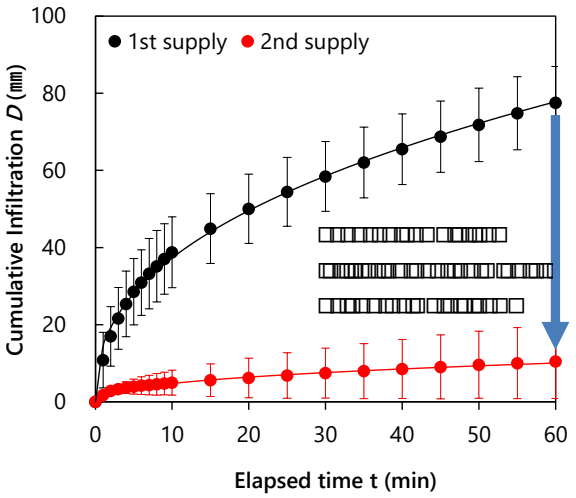

Fig. 3. Furrow infiltration under simplified surge flow irrigation

By wetting the furrow with the first water application under simplified surge flow irrigation, cumulative infiltration over 60 minutes during the second water application on the following day is reduced by approximately 87%.

References: Lee et al. (2025) *PLOS One* 20: e0320775. © Authors 2025
Onishi et al (2021) *Journal of Soil Salinity and Water Quality* 13: 157–163. © Indian Society of Soil Salinity and Water Quality 2021
Figure 2 is reprinted/modified from Lee et al. (2025) under the term of the CC-BY 4.0 license.
https://creativecommons.org/licenses/by/4.0/deed.en
Figure 3 is reprinted/modified from Onishi et al. (2021) with permission.

Three Na^+ exclusion transporters implicated in salt tolerance in quinoa

Salinity severely limits crop production worldwide, whereas major crops remain salt-sensitive. Quinoa (*Chenopodium quinoa* Willd.) is an exceptional crop that combines high nutritional value with remarkable tolerance to harsh environments, including high salinity. Although it is cultivated in extreme environments such as those surrounding the Salar de Uyuni, the mechanisms underlying its salt tolerance remain unclear.

Here, we investigated three genetically distinct quinoa subpopulations, namely the northern highland, southern highland, and lowland, using integrated physiological, transcriptomic, and genomic approaches to elucidate the mechanisms underlying its high salt tolerance.

All 18 quinoa inbred lines representing the northern highland, southern highland, and lowland subpopulations maintained early seedling growth even under high salinity (600 mM NaCl), demonstrating high salt tolerance (Fig. 1). Under these conditions, K^+ accumulation was markedly reduced in the roots but largely maintained in the aerial parts, indicating that quinoa preserves K^+ levels in tissues essential for growth under high salinity. In contrast, Na^+ accumulation in the cotyledons of salt-treated quinoa seedlings tended to be highest in the lowland lines, followed by the northern highland lines, and lowest in the southern highland lines around the Salar de Uyuni (Fig. 2A). Radiolabeled Na^+ uptake experiments further revealed that this variation is attributable to differences in Na^+ uptake into the aerial parts among genotypes (Fig. 2B). Expression of three Na^+ transporter genes, *CqHKT1;1*, *CqHKT1;2*, and *CqSOS1*, did not change markedly in response to high salinity but differed substantially among subpopulations. Sequence polymorphisms in their regulatory regions suggest that genotype-dependent expression may contribute to variation in Na^+ accumulation and salt tolerance. Functional analysis using virus-induced gene silencing showed that suppression of any of these genes increased Na^+ accumulation in the aerial parts, indicating that these transporters play key roles in restricting Na^+ entry into the shoot (Fig. 3A and B).

These findings provide new insight into the Na^+ exclusion mechanism in quinoa and contribute to a better understanding of its remarkable salt tolerance. Elucidating this mechanism offers a valuable foundation for the development of salt-tolerant crops under increasing salinity stress worldwide. In addition, our results highlight the importance of considering genotype-specific variations in transporter gene sequences, which may influence gene expression patterns and transport activity, when investigating Na^+ exclusion mechanisms in quinoa.

Authors: Kobayashi, Y., Murata, Y., Ogata, T., Nagatoshi, Y., Fujita, Y. [JIRCAS], Sugita, R. [Nagoya Univ.], Fujita, M. [RIKEN], Yasui, Y. [Kyoto Univ.]

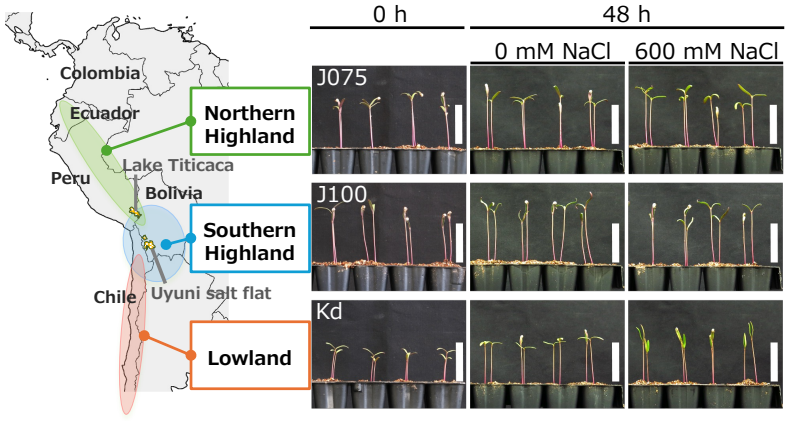

Fig. 1. High salinity does not affect the early seedling growth of quinoa.
(Left) A map showing the regions where quinoa subpopulations classified by genotype are cultivated. (Right) Representative seedlings at 0 h and after 48 h under control or high-salinity conditions. White

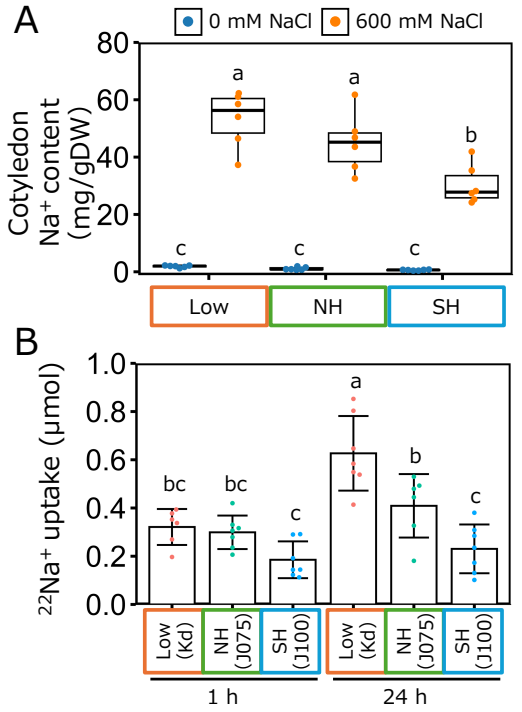

Fig. 2. Quinoa genotype determines aboveground uptake of Na^+.
(A) Na^+ accumulation in the cotyledons of six lines from each quinoa subpopulation after 48 h under control or high-salinity conditions. Different letters indicate significant differences (n = 6, Tukey's HSD test, $p < 0.05$). (B) Uptake of radiolabeled Na^+ into the aerial parts of seedlings after 1 or 24 h in one representative line from each subpopulation. Different letters indicate significant differences (n = 6 or 7; error bars indicate SD; Tukey's HSD test, $p < 0.05$).

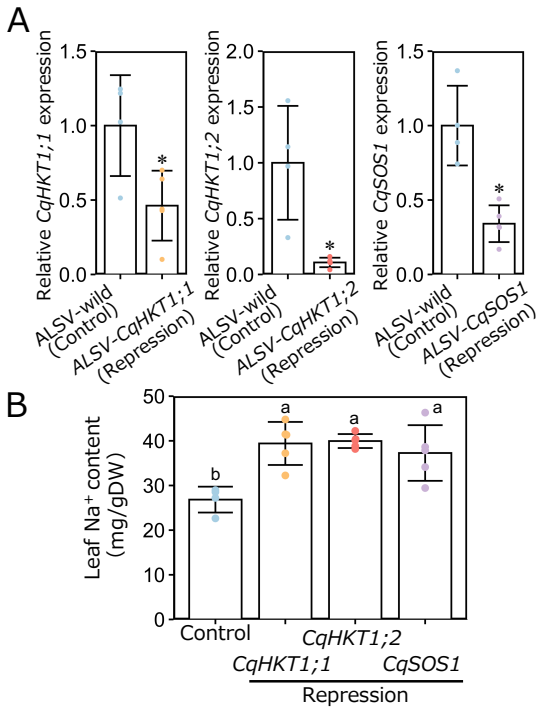

Fig. 3. Three Na^+ transporter genes mediate Na^+ exclusion in quinoa.
(A) Suppression levels of the Na^+ transporter genes *CqHKT1;1*, *CqHKT1;2*, and *CqSOS1* using a virus-induced gene silencing method. Asterisks indicate significant differences (n = 4 or 5; error bars indicate SD; Student's t-test, $p < 0.05$). (B) Na^+ accumulation in leaves of quinoa plants with suppressed expression of each gene under salinity conditions. Different letters indicate significant differences (n = 4 or 5; error bars indicate SD; Tukey's HSD test, $p < 0.05$).

Reference: Kobayashi et al. (2024) *Frontiers in Plant Science* 16: 1597647. © Authors 2025
The figures are modified from Kobayashi et al. (2025).
https://creativecommons.org/licenses/by/4.0/deed.en

Identification of a quantitative locus, *qPA1*, derived from a black rice variety in Laos, which increases phytic acid content in grains

Upland rice is mainly cultivated in the mountainous regions of northern Laos, where soil fertility is low and average yields remain around 2.0 t ha^{-1}. Black rice has traditionally been grown in this region and is an important crop supporting local diets due to its nutritional value and health benefits. However, poor growth under low-fertility conditions remains a major constraint to stable production. Approximately 60–90% of the phosphorus in grains exists as phytic acid (PA), which is sometimes considered to inhibit mineral absorption from a human nutritional perspective. In rice, however, PA serves as the primary phosphorus source during germination and early growth. Particularly under low-phosphorus conditions, PA functions as an important stored form of phosphorus that supports early seedling development. Therefore, PA is a key trait determining crop adaptability, and breeding programs should focus on phosphorus storage traits in grains. The objectives of this study are to identify a quantitative trait locus (QTL) associated with PA content in grains using a genetic population derived from a cross between Kampeng (a black rice variety from Laos) and Non (a stable, high-yielding white rice variety), and to propose a breeding strategy for developing black rice varieties with improved early growth and stable production under low-fertility conditions.

Results indicate that white rice variety Non produces more panicles and thus higher yield potential compared to black rice variety Kampeng (Fig. 1A, B). On the other hand, Kampeng shows higher PA content in grains compared to Non (Fig. 1C). Genetic analysis using an F_2 population derived from a cross between Non and Kampeng identifies a novel QTL, *qPA1*, at the distal end of the short arm of chromosome 1 in both Ishigaki and Vientiane environments, which increases PA content with the Kampeng allele (Fig. 2A). A QTL associated with grain color was detected in *Kala4*, previously reported as a gene controlling the pigmentation of anthocyanins—a health-promoting component—and the Kampeng allele causes grain color to turn black (Fig. 2B). Subsequent studies using F_3 lines derived from the F_2 population confirm that the Kampeng allele enhances PA content by approximately 23% compared to the Non allele (Fig. 3).

Through backcross breeding, the introduction of the Kampeng alleles of *qPA1* and *Kala4* into Non makes it possible to develop a new black rice variety that exhibits high phosphorus supply capacity during germination and early growth, even under low-fertility conditions, while maintaining stable high yield.

Authors: Takai, T., Asai, H., Oo, A.Z., Marui, J., Saito, H. [JIRCAS],
Vilayheuang, K., Phongchanmixay, S. [NAFRI]

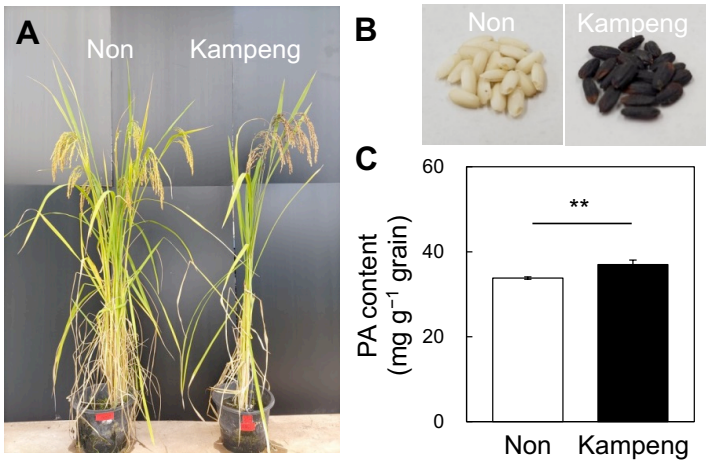

Fig. 1. Phenotype of Non, a stable, high-yielding white rice variety from Laos, and Kampeng, a black rice variety

Plant type (A), grains (B), and PA content in grains (C) of both varieties.
** shows significance at the 1% level by *t*-test.

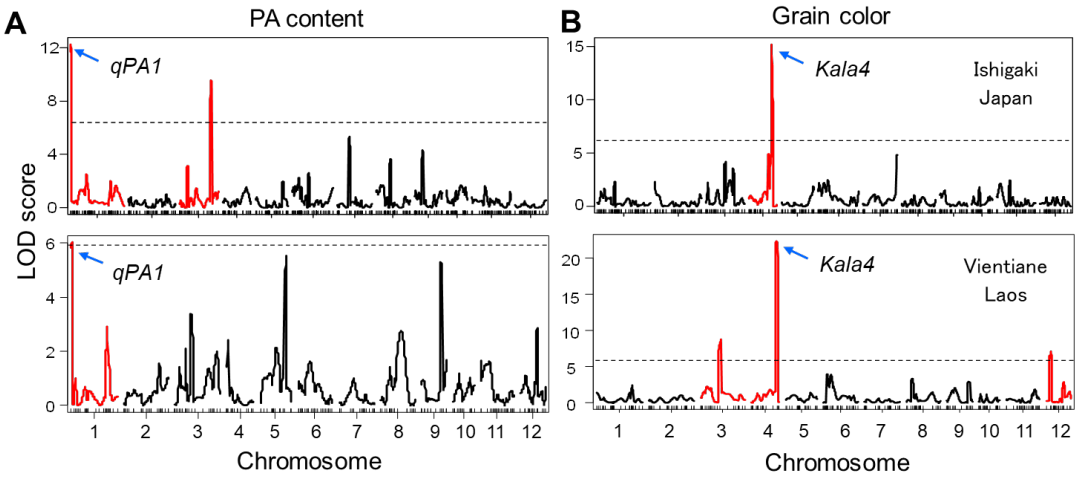

Fig. 2. Genetic analysis of PA content (A) and grain color (B) using an F_2 population derived from a cross between Non and Kampeng

The top and bottom panels show the results in Ishigaki and Vientiane, respectively. The dotted line indicates the threshold for genetic analysis; LOD scores exceeding this threshold are shown in red.

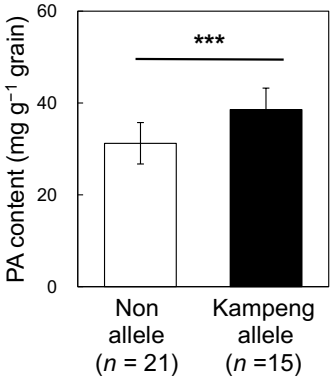

Fig. 3. Comparison of PA content in grains between F_3 lines derived from the F_2 population, where *qPA1* was homozygous for Non and Kampeng, respectively

n indicates the number of lines.
*** shows significance at the 0.1% level by *t*-test.

Reference: Takai et al. (2025) *Frontiers in Sustainable Food Systems* 9: 1620644. © Author(s) 2025
The figures are reprinted/modified from Takai et al. (2025) under the terms of the CC-BY 4.0 license.
https://creativecommons.org/licenses/by/4.0/deed.en

Enhanced dephosphorylation of phytate to inositol in brown-rice *koji-amazake* saccharified with rice-*koji* made with *Aspergillus oryzae* and *Aspergillus luchuensis*

Brown rice provides B vitamins, minerals, and dietary fiber, but its bran layer contains phytate (inositol hexakisphosphate), which binds minerals and can reduce their bioavailability depending on processing and intake conditions. Therefore, brown rice products require processing approaches that enhance nutritional quality. *Koji-amazake* is a sweet, fermented rice drink produced through enzymatic saccharification by rice-*koji* and contains glucose, amino acids, and B vitamins. While *Aspergillus oryzae* is typically used for rice-*koji* production, *Aspergillus luchuensis*, which produces citrate, is also utilized. Phytase and acid phosphatase from both fungi contribute to phytate dephosphorylation. Complete phytate dephosphorylation yields nutritionally important inositol (Fig. 1). This study evaluated acidification resulting from citrate produced by *A. luchuensis*-derived rice-*koji* and quantified phytate dephosphorylation and inositol formation in brown-rice *koji-amazake* saccharified with rice-*koji* derived from *A. oryzae* or *A. luchuensis*, applied either individually or as a mixture.

When brown-rice *koji-amazake* was prepared using 5 g of brown rice (Himenomochi), 10 mL of water, and 3 g of dried rice-*koji* and incubated at 55°C for 8 h, the product made solely with *A. oryzae*-derived rice-*koji* (Condition 1) showed a Brix value of 37.2%, a pH of 5.98, and no detectable citrate (Table 1). Increasing the ratio of *A. luchuensis*-derived rice-*koji* (Conditions 2–5) lowered Brix values and increased citrate content, leading to a decrease in pH (Table 1). In non-fermented mixtures with heat-inactivated *A. oryzae*-derived rice-*koji*, phytate and inositol contents were 652 mg and 2.15 mg per 100 g, respectively, whereas Condition 1 yielded 516 mg of phytate and 9.26 mg of inositol (Fig. 2). Mixed-rice-*koji* Conditions 2–4 significantly enhanced phytate degradation and inositol production compared with Condition 1 (Fig. 2). Condition 5, using only *A. luchuensis*-derived rice-*koji*, produced phytate (158 mg/100 g) and inositol (47.9 mg/100 g) levels similar to those of Condition 4 (Fig. 2).

The incorporation of *A. luchuensis*–derived rice-*koji* effectively promotes phytate dephosphorylation in brown rice-*koji-amazake*, supporting product designs aimed at improving nutritional value. Citrate from *A. luchuensis* acidifies the product, which may enhance microbial stability and broaden flavor options, although consumer preference for sourness should be considered when adjusting formulations. Because this study used commercially available dried rice-*koji* and enzyme activities vary among fungal strains, the practical application of these findings requires evaluating strain-specific enzymatic properties of the rice-*koji* used.

Authors: Marui, J. [JIRCAS], Shiraishi, Y., Takeura, M. [Bio'c],
Shompoosang, S., Varichanan, P. [IFRPD], Boulom, S. [NUOL]

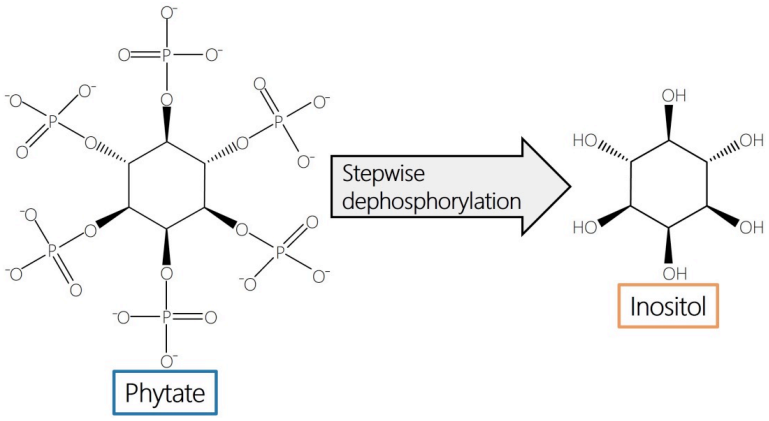

Fig. 1. Chemical structures of phytate and inositol formed through its stepwise dephosphorylation

Table 1. Brix values, citrate contents, and pH of brown-rice *koji-amazake* saccharified with rice-*koji* made with *Aspergillus oryzae* and *Aspergillus luchuensis*

	Ratio of rice-*koji* derived from *A. oryzae* and *A. luchuensis* (%)				
Conditions	*A. oryzae*	*A. luchuensis*	Brix (%)*	Citrate (%)*	pH*
1	100	0	37.2 (0.17)	Not detected	5.98 (0.04)
2	75	25	36.7 (0.24)	0.18 (1.6)	4.74 (0.02)
3	50	50	36.0 (0.12)	0.26 (1.4)	4.17 (0.03)
4	25	75	35.6 (0.19)	0.44 (2.2)	3.88 (0.05)
5	0	100	35.4 (0.42)	0.56 (1.6)	3.68 (0.05)

*Values represent means of three replicates, with standard deviations in parentheses.

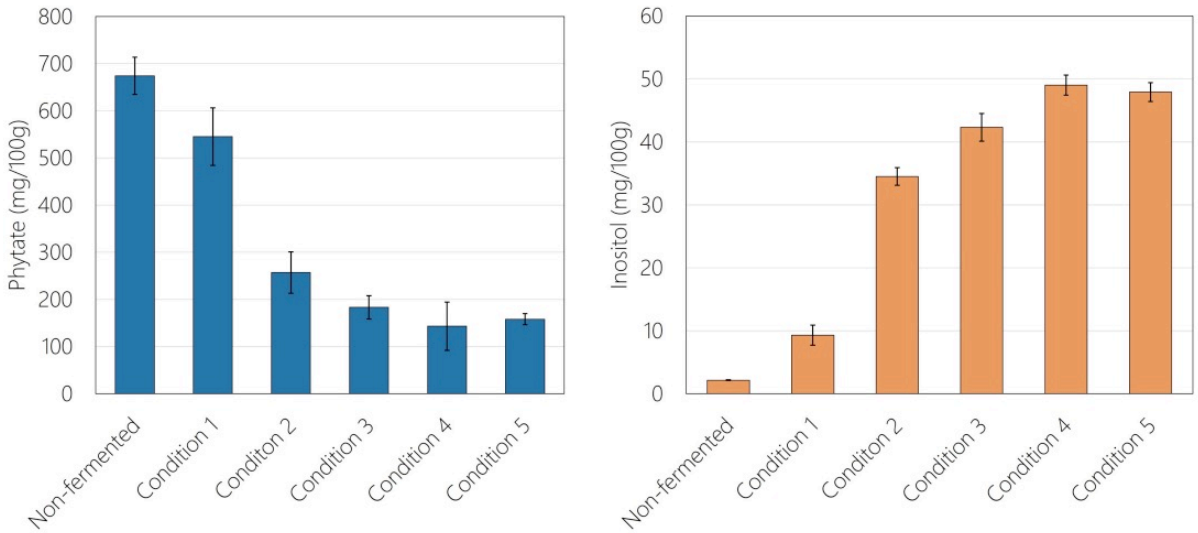

Fig. 2. Phytate and inositol contents in brown-rice *koji-amazake* saccharified with rice-*koji* made with *Aspergillus oryzae and Aspergillus luchuensis*

Values represent means of three replicates obtained from the pre-fermentation sample and from brown-rice *koji-amazake* prepared under Conditions 1–5 shown in Table 1, with error bars indicating standard deviations.

Reference: Marui et al. (2025) *Food Science and Technology Research* 31: 147–153.
© The Japanese Society for Food Science and Technology 2025
The figures and table are reprinted/modified from Marui et al. (2025) under the terms of the CC-BY 4.0 license.
https://creativecommons.org/licenses/by/4.0/deed.en

Rearing cost analysis of natural enemy insects for fall armyworm control in Thailand

In Thailand, efforts to control the fall armyworm (*Spodoptera frugiperda*) have raised concerns about insecticide resistance, prompting the establishment of an integrated pest, disease, and weed management (IPM) system. As part of this initiative, the Department of Agriculture has promoted biological control through mass-rearing and distribution of multiple natural enemy species. However, the use of natural enemies remains limited, and their higher costs compared to chemical pesticides are major obstacles. Systematic knowledge of rearing costs is still insufficient, and variation in rearing scales reported in previous studies has hindered generalization. This study develops a cost estimation model that explicitly links release area to rearing scale, enabling evaluation of economic feasibility.

Rearing techniques at the Plant Protection Research and Development Office (PPRDO) of the Department of Agriculture were reviewed. Based on information for each operational step, required material quantities and costs were estimated from the maize area targeted for pest control. The natural enemies examined were the egg parasitoid wasp *Trichogramma pretiosum* and three predatory insects: *Eocanthecona furcellata* (stinkbug), *Sycanus versicolor* (assassin bug), and *Proreus simulans* (brown earwig). Assuming small-scale rearing at the maximum production capacity of a single worker, costs were estimated for each species. Results showed that average rearing cost per hectare declines with increasing release area due to the dilution of fixed costs (Fig. 1). For *T. pretiosum*, *E. furcellata*, and *S. versicolor*, water, utilities, and labor account for a large share of total costs, resulting in pronounced scale-related reductions (Fig. 1, Table 1). At maximum production scale, the rearing cost of *T. pretiosum* does not substantially exceed that of emamectin benzoate 5% water-dispersible granules, which are widely used in Thailand (≈9 USD ha^{-1}), suggesting it could partially substitute for chemical control (Fig. 1B, Table 1).

The cost estimation approach is applicable to other species and regions, providing a basis for the economic assessment of biological control. The model is simplified for laboratory-level estimation, based on standardized production periods, single-worker capacity, and assumed release densities, and may require adjustment for specific objectives. The labor and costs associated with release operations, as well as the use and production of natural enemies during pest-free periods, also warrant examination. As this analysis relies solely on PPRDO data, further data collection and validation are needed. Beyond rearing costs, further research on control efficacy, optimal release densities, and integration with other control methods is needed to support practical implementation.

Authors: Kusano, E., Kobori, Y. [JIRCAS]

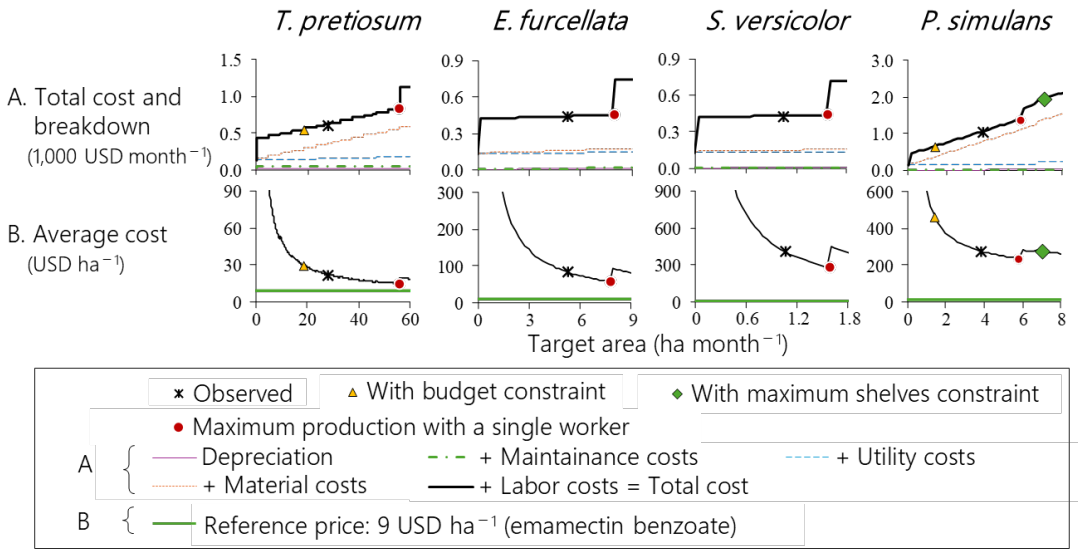

Fig. 1. Total and average costs of rearing natural enemy insects

Panel A shows stacked line charts of model-estimated costs, with observed values overlaid. Panel B shows line charts of model-estimated costs, with the reference price (9 USD ha^{-1}) indicated for comparison. "Observed" represents results from PPRDO interviews. "With budget constraint" indicates the level of subsidies for rearing natural enemy insects, and "With maximum shelves constraint" refers to the largest rearing scale that can fit in the room given shelf availability. Symbols were omitted when estimated values under budget or shelf constraints were excessively large. The target area was determined by the number of natural enemies used and the release density. Estimated costs include materials for release but exclude labor costs.

Table 1. Rearing cost breakdown at maximum single-worker scale

Item	*T. pretiosum*	*E. furcellata*	*S. versicolor*	*P. simulans*
Basic assumptions and results				
Target area (ha month^{-1})	55.93	7.93	1.59	5.82
Release density	62.5	3,125	3,125	10,000
Cost breakdown				
Total cost (USD month^{-1})	820	455	437	1,377
Average cost per NE (USD unit^{-1})	0.235	0.018	0.088	0.024
Average cost per area (USD ha^{-1})				
Total	14.67	57.40	275.73	236.77
Material cost	6.71	3.70	10.13	161.42
Depreciation	0.34	1.46	4.35	3.42
Maintenance cost	0.57	0.18	0.89	0.49
Labor cost	4.81	35.73	178.68	48.72
Utility cost	2.22	16.33	81.67	22.72

Values represent rearing costs at the maximum production scale of a single worker. NE = natural enemy. Release density indicates the number of NEs released per crop field. Units: *Trichogramma pretiosum* = strips of 3,571 *Corcyra cephalonica* eggs parasitized; predatory NEs = number of insects. Exchange rate: USD 1.00 = 35.29 Thai Baht (average for 2024).

Reference: Kusano et al. (2026) *CABI Agric Biosci* 7: 0006. © Authors 2026

The figure and table are reprinted/modified from Kusano et al. (2026).

Long-term preservation of genetic resources in the giant freshwater prawn by germ cell cryopreservation

Cryopreservation of germ cells is a promising approach for preserving the entire genetic background of crustaceans, for which cryopreservation of gametes and early embryos remains difficult. In aquaculture, repeated use of limited broodstock lines over time can reduce genetic diversity and increase vulnerability to disease, making the development of reliable genetic resource preservation technologies increasingly important for sustainable production.

The giant freshwater prawn (*Macrobrachium rosenbergii*), native to Southeast Asia, is one of the most economically important freshwater aquaculture species. However, repeated use of limited lines raises concern about future loss of genetic diversity. To address this issue, this study developed a method for cryopreserving germ cells of the giant freshwater prawn and evaluated suitable cryoprotectants and freezing conditions for long-term preservation.

The study showed that germ cells of the giant freshwater prawn could be identified using a commercially available anti-Vasa antibody and efficiently selected on the basis of cell diameter (8–10 μm) alone. Among the cryoprotectants tested, 10% dimethyl sulfoxide (DMSO) gave better recovery and survival rates than glycerol or magnesium chloride. In addition, ultra-rapid freezing outperformed slow freezing in maintaining higher recovery and survival rates during long-term storage. When combined with 10% DMSO, ultra-rapid freezing maintained high recovery and survival rates even after more than 6 months of storage in liquid nitrogen.

This is the first report establishing germ-cell cryopreservation in freshwater prawns. The results indicate that genetic resources of the giant freshwater prawn can be preserved long term in a space-saving manner without continuous maintenance of live individuals. The same cryopreservation condition was also effective in marine penaeid shrimp reported previously, suggesting broader applicability to crustacean germ cells. Although direct regeneration of individuals from cryopreserved germ cells has not yet been achieved, further development of related technologies, such as germ-cell transplantation, which has already been applied in finfish species, will be necessary. This study therefore provides a foundation for future breeding and conservation of valuable aquaculture lines.

Authors: Okutsu, T. [JIRCAS], Rakbanjong, N., Wonglapsuwan, M. [Prince of Songkla Univ.], Miwa, M. [Tokyo Univ. of Marine Sci. and Tech.], Shikina, S. [National Taiwan Ocean Univ.]

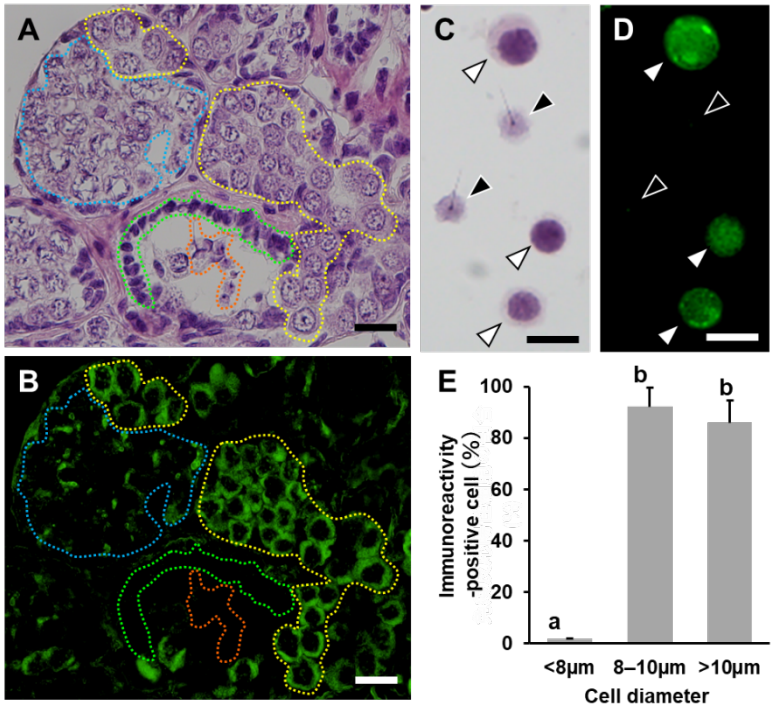

Fig. 1. Identification of germ cells in the giant freshwater prawn by immunostaining
(A) HE-stained testis section. (B) Immunostained image of the same section. (C) Bright-field image of dissociated testicular cells. (D) Fluorescence image corresponding to (C). (E) Percentage of immunopositive cells in each cell-size class. Germ cells showed strong positive immunoreactivity to anti-Vasa antibody, and the 8–10 μm fraction showed the highest positive rate. Different letters indicate significant differences ($p < 0.05$, Tukey–Kramer test).

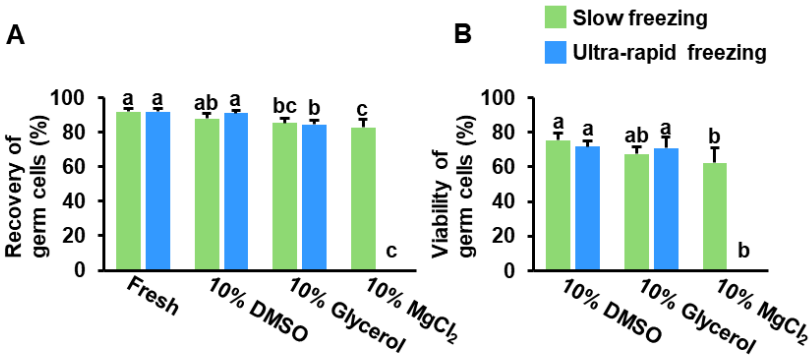

Fig. 2. Examination of the optimal cryoprotectant
Germ-cell recovery (A) and survival (B) after slow freezing and ultra-rapid freezing using 10% DMSO, 10% glycerol, or 10% $MgCl_2$ as cryoprotectants. In both freezing methods, 10% DMSO gave the highest recovery and survival rates. Different letters indicate significant differences ($p < 0.05$, Tukey–Kramer test).

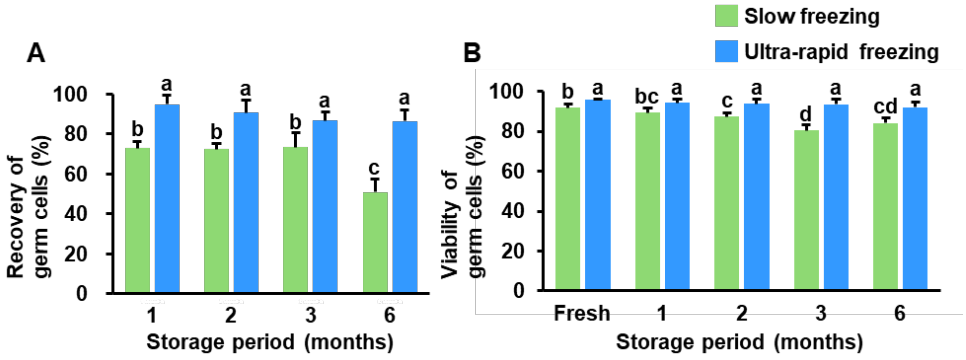

Fig. 3. Germ-cell recovery and survival after long-term cryopreservation
Recovery (A) and survival (B) of germ cells after storage in liquid nitrogen using slow freezing or ultra-rapid freezing with 10% DMSO. Ultra-rapid freezing gave higher values than slow freezing, even after 6 months. Different letters indicate significant differences ($p < 0.05$, Tukey–Kramer test).

Reference: Okutsu et al. (2025) *Cryobiology* 119: 105242. © Authors 2025
The figures are reprinted/modified from Okutsu et al. (2025).

Life history traits of the small freshwater shrimp, *Macrobrachium lanchesteri* species complex, in Northeast Thailand and its implications on fisheries management

Lanchester's Freshwater Prawn *Macrobrachium lanchesteri* species complex (Fig. 1) is an important freshwater crustacean resource in the inland Indochinese Peninsula, comparable to the Giant Freshwater Prawn (*M. rosenbergii* and *M. dacqueti*). Its sustainable use requires scientific information on life history, including when it spawns and how long it takes for individuals to become available to fisheries. While maturation and spawning of this species have been studied in the Ayeyarwady River System, central Myanmar, and Northern Thailand, no information was available on its recruitment and growth. In this study, specimens were collected monthly over one year from an oxbow lake in Ubon Ratchathani Province, Northeast Thailand, where shrimp fisheries operate year-round. The specimens were analyzed for individual size and maturity status to elucidate their growth, maturation, spawning, and recruitment to the fishery stock. Fisheries management practices were explored based on the life history findings to ensure sustainable use of this shrimp stock. This shrimp is a purely freshwater species that does not migrate long distances from their habitat.

The smallest mature female (carrying eggs under the abdomen (Fig. 1A) or having developed ovaries (Fig. 1B)) collected in this study was 4.6 mm in carapace length (red solid line in Fig. 2). While the species complex spawns year-round, peak spawning occurs during mid-rainy season from June to August (red shading in Fig. 3), and spawning stagnates during the dry season from November to December (blue shading in Fig. 3). Hatched shrimp begin appearing in catches as small immature individuals from September to November (recruitment; gray shading in Fig. 2), and they mature and spawn in less than a year after hatching, between March and May of the following year (red shading at the bottom of Fig. 2). The no-fishing period regulating commercial fisheries of all aquatic animals (artisanal fisheries excluded) in the region coincides with the spawning peak of the shrimp, confirming the effectiveness of this regulation in conserving adult shrimp. Furthermore, since small immature shrimp begin joining fisheries stocks around September and mature by the following rainy season, avoiding their capture during this period is suggested as an additional effective resource management strategy.

Life history information, including peak spawning period, size range and period of major recruitment to the fisheries stock, and duration until maturation, helps design effective management measures for sustainable use of small freshwater shrimp resources in the inland Indochinese Peninsula. Juvenile recruits may be conserved through mesh size regulations and shelter conservation, in addition to reducing total fishing pressure.

Authors: Saito, M., Honda, S. [JIRCAS],
Grudpan, C., Grudpan, J., Jutagate, A., Jutagate, T. [Ubon Ratchathani Univ.]

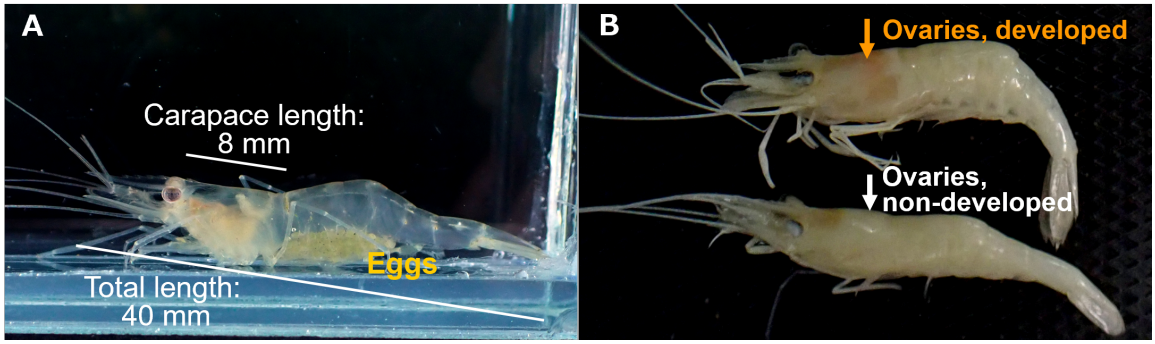

Fig. 1. Female individuals of the small freshwater shrimp, *Macrobrachium lanchesteri*

A: Live specimen carrying eggs (light yellow part) under the abdomen. B: Fixed specimens with different levels of ovary maturity. Developed ovaries are the dark-orange parts visible through the shell (carapace).

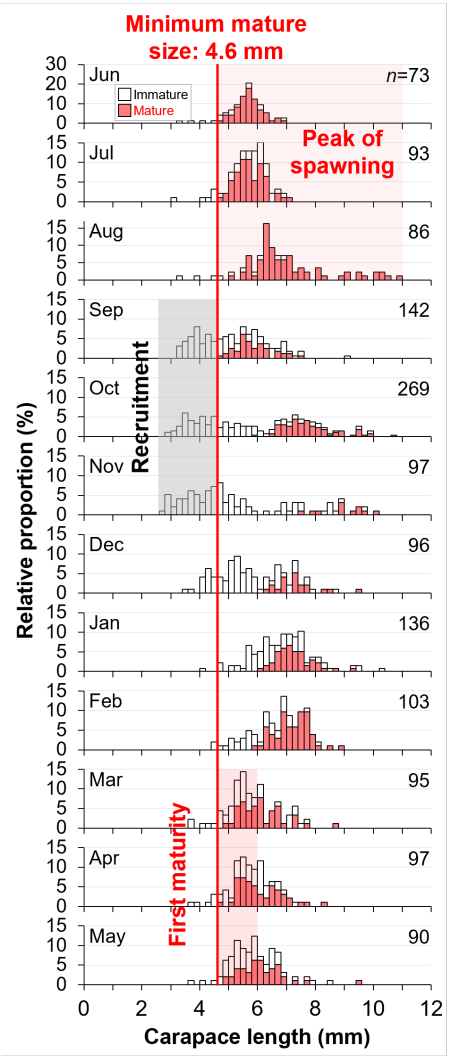

Fig. 2. Monthly changes in carapace length-frequency distribution and maturation in female *M. lanchesteri* species complex

The shaded parts indicate representative life history events and its size range. The red solid line indicates the minimum mature size (4.6 mm carapace length) of females elucidated in this study. Please see Fig. 3 for the criteria for identifying mature females.

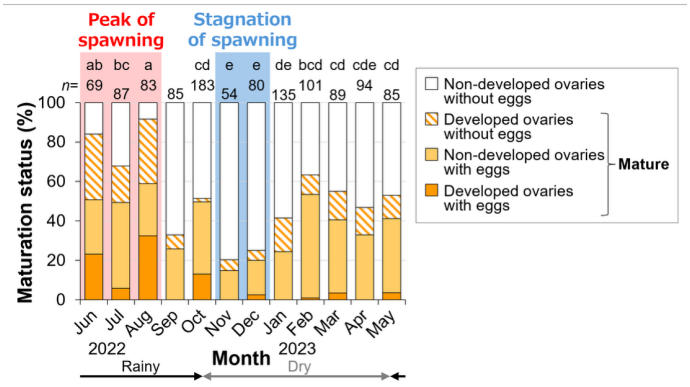

Fig. 3. Monthly changes in the maturation status of female *M. lanchesteri* species complex

Data relating to individuals larger than the minimum maturation size are shown in the graph (see Fig. 2). Different letters above the bars indicate significant differences in the monthly proportions of mature females (Fisher's exact test, $p<0.05$). September samples were excluded from the testing because the shrimp may have dropped eggs due to the effects of flooding.

Reference: Saito et al. (2025) *Fisheries Research* 292: 107569. © Authors 2026
The figures are modified from Saito et al. (2025) under the terms of the CC-BY 4.0 license.
https://creativecommons.org/licenses/by/4.0/deed.en

Seedling production technology for gametophytes of the red alga *Asparagopsis taxiformis* utilizing its life cycle

The red alga *Asparagopsis taxiformis* has recently attracted attention as a promising seaweed for reducing methane emissions from ruminant livestock due to its high content of bromoform, a compound known to inhibit microbial methanogenesis. However, the practical implementation of its aquaculture requires the establishment of a stable and efficient seedling supply system.

A. taxiformis has a heteromorphic life cycle that consists of sporophyte (2n) and gametophyte (n) phases. While sporophytes are too small to be cultured in marine environments, gametophytes are applicable to marine farming, which is less costly and suitable for large-scale cultivation. This study focuses on the alternation of generations in *A. taxiformis*, to develop techniques for seedling production suitable for sea-based cultivation by inducing spore release from sporophytes and promoting the growth of gametophytes.

The results demonstrate that sporophytes can be stably maintained at 20°C under a 12 h light: 12 h dark photoperiod, but maturation and tetraspore release are effectively induced under either elevated temperature (25°C) or short-day conditions (8 h light: 16 h dark). These two factors act independently, yet exhibit a synergistic effect when combined, reducing the time required for initial spore release to approximately 11 days. Under other conditions, neither maturation nor spore release was observed, indicating that precise environmental control is essential for reliable seed production.

Furthermore, the growth of gametophytes derived from spores is significantly enhanced under aerated culture conditions. Over a four-week period, the daily growth rate increased from 4.72% under static conditions to 6.86% with aeration. Aerated cultures also showed more pronounced development of upright axes, lateral branches, and basal structures. In addition, the bromoform content per unit dry weight was substantially higher under aeration, indicating improved functional quality.

These findings provide a practical foundation for low-cost, large-scale marine cultivation of *A. taxiformis* by enabling stable gametophyte seedling production independent of land-based systems.

Authors: Matsuda, R. [JIRCAS], Kuwano, K. [Nagasaki Univ.]

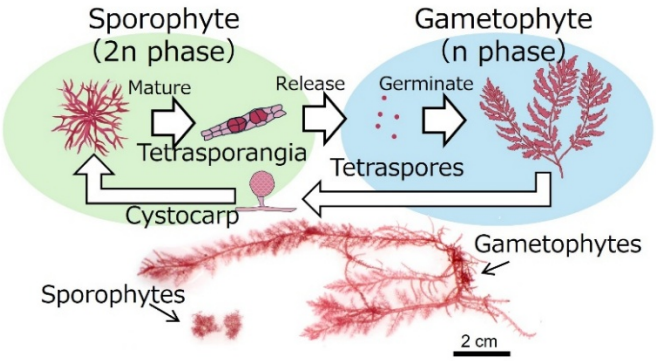

Fig. 1. Life cycle of *Asparagopsis*

The red alga *Asparagopsis taxiformis* has a life cycle in which the sporophyte (2n phase) and gametophyte (n phase) alternate generations. Upon maturation, the sporophyte forms tetrasporangia and releases tetraspores, which upon germination develop into gametophytes. The gametophytes reproduce sexually, forming a cystocarp through fertilization, which then develops into a sporophyte.

Water Temp	Light: Dark cycle	Spore Release
20 °C	L:D 12 h: 12 h	×
25 °C	L:D 12 h: 12 h	○
30 °C	L:D 12 h: 12 h	×
20 °C	L:D 14 h: 10 h	×
20 °C	L:D 12 h: 12 h	×
20 °C	L:D 10 h: 14 h	×
20 °C	L:D 8 h: 16 h	○

Table 1. Conditions for spore release

This table indicates whether spore release occurred (○) or did not occur (×) when *A. taxiformis* sporophytes were cultured for 21 days under different temperature and photoperiod conditions. L:D denotes the light period (L) and dark period (D); for example, L:D 12 h:12 h indicates a photoperiod of 12 hours light and 12 hours dark.

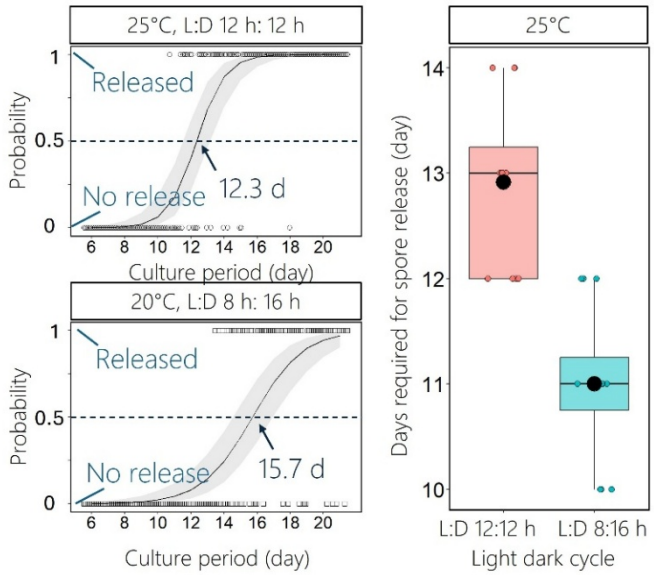

Fig. 2. Effects of temperature and photoperiod on spore release

The left panels show the probability of spore release (1 = occurred, 0 = not occurred) when sporophytes were cultured under a water temperature of 25°C or a photoperiod of 8 h: 16 h L:D. Arrows and shaded areas indicate the 50% spore release day and the 95% confidence interval estimated by binomial logistic regression. The right panel shows box plots of days to first spore release at 25°C under different photoperiods. ● = mean. (n = 12)

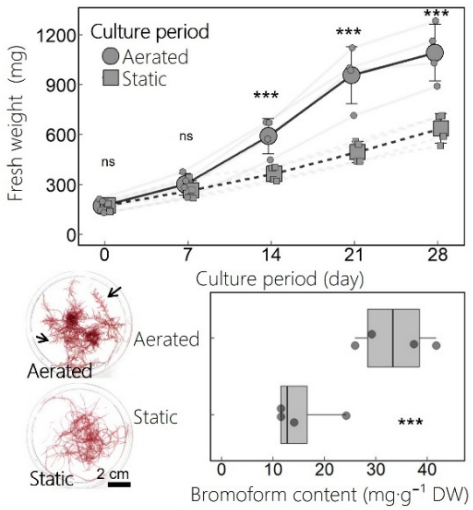

Fig. 3. Efficient cultivation method for gametophytes

Growth curves (upper graphs), morphology at day 28 (lower photos), and bromoform content per dry weight (lower graphs) of gametophytes cultured under aerated or static conditions. Arrows indicate the development of erect thalli with lateral branches. Fresh weight and bromoform content were compared using a generalized linear model. ns: $p > 0.05$; ***: $p < 0.001$ (n = 4)

Reference: Matsuda and Kuwano (2025) *Marine Biotechnol* 27:115. © Authors 2025
The figures are reprinted/modified from Matsuda and Kuwano (2025) under the terms of the CC-BY 4.0 license.
https://creativecommons.org/licenses/by/4.0/deed.en

Development of a low-cost intermediate nursery system for tropical oyster aquaculture

High mortality of early-stage oyster spat remains a central obstacle to the growth of tropical oyster aquaculture, particularly in mangrove-influenced estuaries where environmental fluctuations, hypoxia, turbidity, and biofouling impose severe stress on juvenile oysters. Conventional solutions such as land-based tank rearing and large commercial floating upweller system units can stabilize early growth but are prohibitively expensive and labor-intensive for the small-scale farmers who dominate production in regions like Peninsular Malaysia. To provide a practical alternative, this study developed a low-cost, forced-flow nursery upweller that can be constructed entirely from commercially available materials—including a plastic bucket, mesh trays, and a compact submersible pump—while remaining lightweight, portable, and easy to maintain under field conditions.

A 14-day field experiment in the upper Merbok estuary compared three rearing methods—a conventional net cage, a net cage with aeration, and the improved upweller system. During the trial, water temperatures were 30–32°C, salinity stayed around 24–25, and chlorophyll-a levels reached up to 27 µg/L, providing optimal feeding conditions. The upweller ran stably without pump clogging despite moderate biofouling, and its simple design enabled easy lifting, cleaning, and reinstallation by a person. Growth results showed advantages: 80% of oysters in the upweller formed new shell edges, compared with 47% and 57% in the other treatments. Additionally, 23% of oysters in the upweller exceeded 18 mm in shell length, and digestive-gland phytopigments were significantly higher ($p < 0.05$), indicating enhanced feeding efficiency under forced water exchange.

These findings demonstrate that the forced-flow upweller provides a highly effective, accessible, and scalable solution for the intermediate nursery phase in tropical estuarine aquaculture. By stabilizing early growth and reducing mortality risk, the system helps lower seed costs and improves income reliability for small-scale farmers, while also reducing labor demands through simplified maintenance. Although the device currently requires a power source, future improvements—including solar-powered operation and potential integration with IoT-based environmental monitoring—could further enhance operational resilience in dynamic mangrove ecosystems. Overall, the developed nursery upweller represents a promising technology that supports sustainable expansion of oyster aquaculture in Southeast Asia and other tropical estuarine regions.

Authors: Yurimoto, T. [JIRCAS]

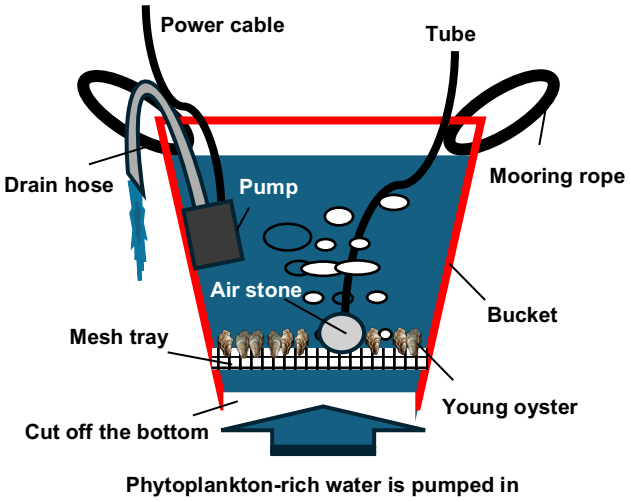

Fig. 1. Upwelling nursery system schematic
Built with low-cost materials, the simplified design enables easy cleaning and adaptation to brackish mangrove areas.

Fig. 2. Test operation of the intermediate nursery system
(a) The waterproof box holds the power cables and pump timer. (b) A mesh tray with juveniles is set at the bottom of the unit.

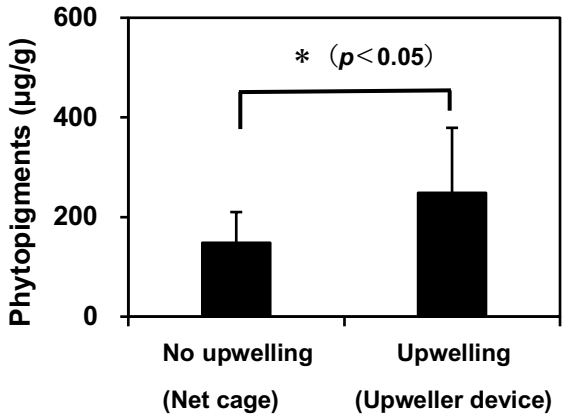

Fig. 3. Digestive-gland chlorophyll comparison
Values reflect feeding; groups differ (*t*-test, $p < 0.05$).

Fig. 4. Young oyster after two weeks
New shell growth appeared only in the system group.

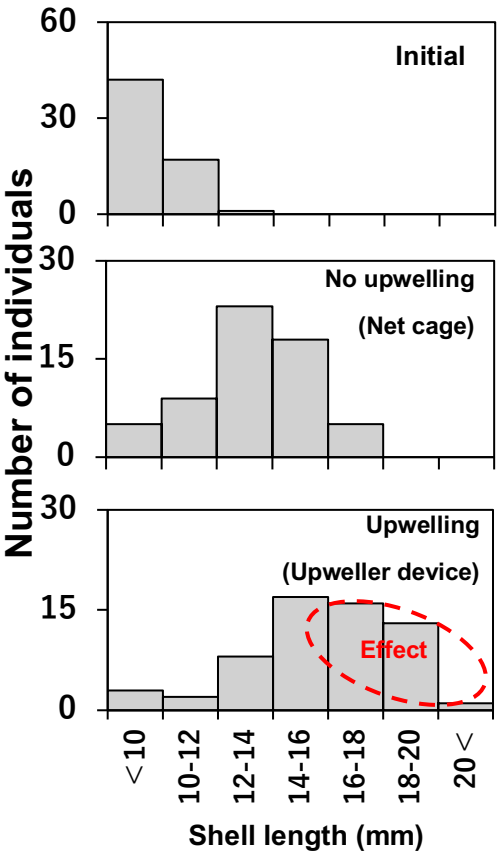

Fig. 5. Two-week comparison of young oyster shell-length distributions
The shell-length distribution of the system group shifted toward larger size classes after two weeks (χ^2 test, $p < 0.01$).

Reference: Yurimoto et al. (2025) *Aquatic Sciences and Engineering* 40(4): 262–271. © Authors 2025
The figures are reprinted/modified from Yurimoto et al. (2025) under the term of the CC BY-NC 4.0 license.
https://creativecommons.org/licenses/by-nc/4.0/deed.en

Soil type–specific sorghum cultivation strategies for maximizing yield and net return in the Sudan Savanna

To meet the rapidly increasing food demand in Sub-Saharan Africa (SSA), improving agricultural productivity in the region is essential. In countries across the Sudan Savanna, the largest sorghum-producing region in SSA, agricultural recommendations are being revised. However, differences in soil types—which significantly influence sorghum yield—have not yet been taken into account.

Therefore, this study aims to identify optimal combinations of nitrogen (N) application rate, planting density, and variety (i.e., optimal cultivation practices) that maximize sorghum yield and net return from fertilization in three dominant soil types in the Sudan Savanna: Lixisols (LX), characterized by a deep effective soil depth (~100 cm); Plinthosols with medium effective depth (~50 cm; PT); and Plinthosols with shallow effective depth (~25 cm; PX).

The optimal cultivation practices identified through two years of field experiments were as follows (Table 1):

LX: 74 kg N ha^{-1}, 5.6 plants m^{-2}, Sariaso14

PT: 74 kg N ha^{-1}, 8.3 plants m^{-2}, Kapelga

PX: 37 kg N ha^{-1}, 3.1 plants m^{-2}, Kapelga

As expected, these practices differed depending on soil type. Current agricultural recommendations for sorghum in each country generally prescribe an N application rate of around 30 kg ha^{-1} regardless of soil type. However, increasing the N application rate in LX and PT can improve both yield and net return. Based on fertilizer prices and farm-gate prices of sorghum in Burkina Faso from 2010 to 2022, a period during which prices fluctuated significantly, the net returns from fertilization under the optimal practices was calculated. The average net returns followed the order LX > PT > PX, reflecting differences in effective soil depth (Fig. 1). The economic robustness of the optimal cultivation practices also differed among soil types. In LX and PT, net returns from fertilization remained positive even under high fertilizer prices, whereas in PX, where the effective soil depth is shallow, net returns could become negative (Fig. 1).

These findings can be used to improve existing agricultural recommendations for sorghum in countries across the Sudan Savanna, making them more fertilizer-efficient. However, sorghum yields and net returns from fertilization in this study were obtained under fertilization practices recommended by INERA: a basal application immediately after sowing, followed by top-dressing at 4 and 6 weeks after sowing. Therefore, even with the same total N application rate, different application timings or frequencies may not yield the same results.

Authors: Ikazaki, K., Iseki, K. [JIRCAS], Nagumo, F. [JICA], Simporé, S., & Barro, A. [INERA]

Table 1. Effects of nitrogen application rate, planting density, and variety on sorghum yield and net returns from fertilization across soil types

	Sorghum yield (kg ha^{-1})			Net return (10^3 FCFA ha^{-1})		
	LX	PT	PX	LX	PT	PX
A: Nitrogen application rate[1)]						
37 kg ha^{-1}	**1098 a**	**619 a**	691	**55 a**	**3 a**	25
74 kg ha^{-1}	**1660 b**	**1049 c**	857	**136 b**	**60 b**	33
111 kg ha^{-1}	**1724 b**	**820 b**	782	**126 b**	**–4 a**	–3
B: Planting density						
3.1 hills m^{-2}	**1332 a**	**696 a**	784	**80 a**	**–2 a**	24
5.6 hills m^{-2}	**1661 b**	**828 ab**	762	**136 b**	**19 ab**	17
8.3 hills m^{-2}	**1490 ab**	**975 b**	774	**101 ab**	**43 b**	14
C: Variety[2)]						
Kapelga	1453	870	**853 b**	100	28	**34 b**
Sariaso14	1535	800	**691 a**	112	12	**2 a**

Results from a two-year field experiment (a normal rainfall year and a low rainfall year) conducted in central Burkina Faso, where representative geology, topography, and soils of the Sudan Savanna are distributed. LX denotes Lixisols with a deep effective soil depth (~100 cm); PT denotes Plinthosols with medium effective depth (~50 cm); and PX denotes Plinthosols with shallow effective depth (~25 cm). Values represent means for each treatment. Different letters indicate significant differences ($p < 0.05$) in mean yield or net returns from fertilization within each soil type and factor (A, B, and C). Letters are omitted when differences are not significant. No interaction was observed among factors A, B, and C.

[1)] Phosphorus (23 kg ha^{-1} as P_2O_5) and potassium (14 kg ha^{-1} as K_2O) were applied as basal fertilizer in all treatments. [2)] In LX, both yield and net returns from fertilization were significantly higher ($p < 0.05$) for Sariaso14 than for Kapelga in the normal rainfall year, and because normal rainfall years occur more frequently than low rainfall years, Sariaso14 was selected as the optimal variety. In contrast, in PT, no significant differences in yield or net return from fertilization were observed between Sariaso14 and Kapelga; however, Kapelga was selected as the optimal variety because of its superior palatability and storability compared with Sariaso14.

1 FCFA = 0.28 JPY (December 2025).

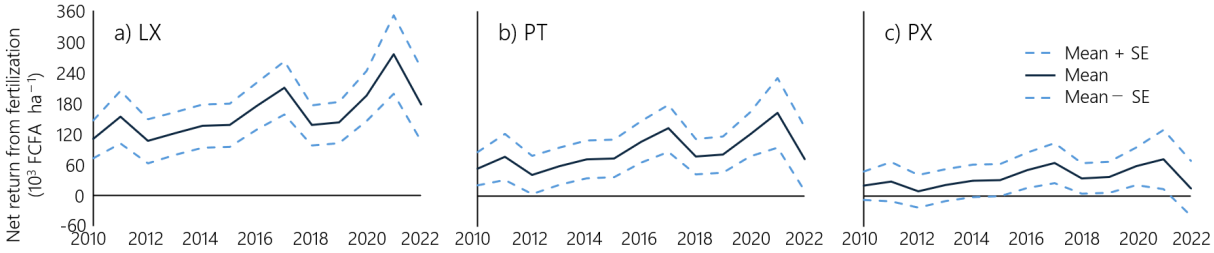

Fig. 1. Net returns from fertilization under optimal cultivation practices across soil types from 2010 to 2022

LX, PT, and PX are defined as in Table 1. In LX and PT, even during the period from 2010 to 2022 when prices fluctuated substantially, the value of the mean minus one standard error (SE) remained consistently positive. In contrast, in PX, where the effective soil depth is shallow, the mean minus one SE became negative under high fertilizer prices, indicating the potential for economic loss due to fertilization.

Reference: Ikazaki et al. (2025) *Soil Sci. Plant Nutri.* 71: 724–735. © Authors 2025
The table and figure are modified from Ikazaki et al. (2025) under the terms of the CC-BY 4.0 license.
https://creativecommons.org/licenses/by/4.0/deed.en

Cowpea genetic resources tolerant to both drought and excess soil moisture and their root morphological adaptations

In the dry savannas of West Africa, smallholder farming systems depend heavily on rainfall and are therefore highly vulnerable to climate variability and climate change. In recent years, rainfall patterns have become increasingly erratic, causing not only drought but also temporary waterlogging following extreme rainfall events. Such fluctuations in soil moisture pose serious risks to crop production. In legumes such as cowpea, excess soil moisture leads to oxygen deficiency in the root zone, which suppresses plant growth and reduces yield. Developing crop varieties that can tolerate both drought and excess soil moisture has therefore become an urgent priority.

In collaboration with the International Institute of Tropical Agriculture (IITA), we evaluated 99 cowpea genetic resources, including 45 ancestral wild accessions collected from diverse environments and 54 cultivated accessions, mainly from the cowpea core collection. Stress tolerance was comprehensively assessed under both drought and excess soil moisture conditions using multiple physiological and growth indicators. Under drought conditions, SPAD values and chlorophyll fluorescence were used to evaluate leaf physiological status, while under excess soil moisture conditions, SPAD values and aboveground growth were used to assess plant performance.

As a result, ten accessions showing tolerance to both drought and excess soil moisture were identified (Fig. 1). Notably, nine of these accessions were ancestral wild relatives, indicating that wild genetic resources retain valuable stress tolerance traits that are rarely found in cultivated varieties. Anatomical analyses revealed distinct root morphological responses associated with tolerance. Under excess soil moisture conditions, tolerant accessions increased the formation of root aerenchyma, facilitating internal oxygen transport and alleviating oxygen deficiency in the root zone (Fig. 2). In contrast, under drought conditions, they increased the proportion of vascular tissues in the stele, enhancing water transport efficiency from roots to shoots.

These results demonstrate that multi-indicator evaluation can effectively identify genetic resources tolerant to contrasting stresses such as drought and excess soil moisture. The tolerant genetic resources and their associated root traits identified in this study provide promising targets for breeding cowpea varieties adapted to future climates characterized by increasingly variable rainfall conditions.

Authors: Iseki, K. [JIRCAS], Olaleye, O. [IITA]

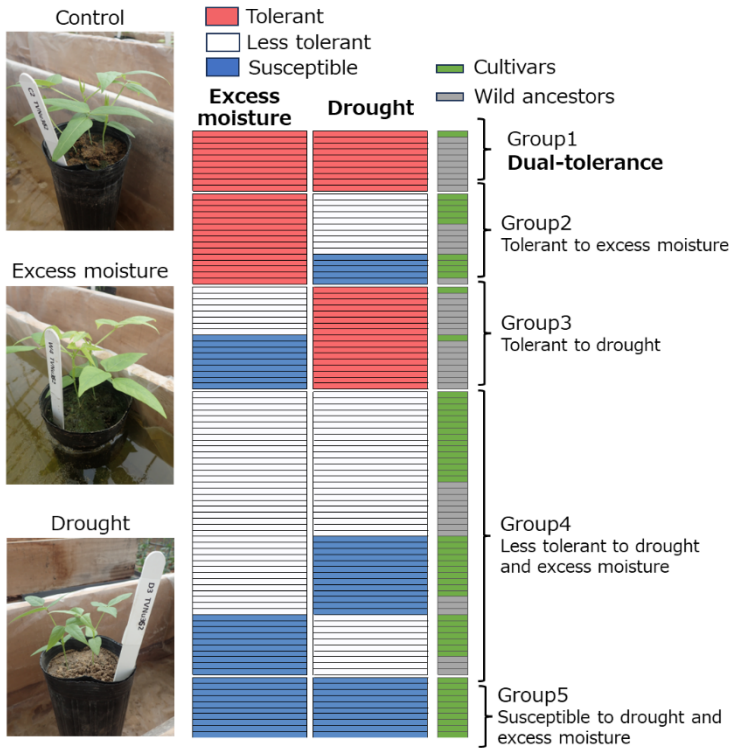

Fig. 1. Drought and excess soil moisture tolerance in 99 cowpea genetic resources

Plants were grown in 20-cm pots under normal moisture (20–25%) for two weeks. Excess moisture was imposed by immersing pots to an 18-cm depth (40–50%), while drought stress was applied by withholding irrigation (<10%). Based on responses three weeks after treatment, accessions were classified into five groups. Red, white, and blue indicate strong, moderate, and weak tolerance, respectively. Cultivated varieties are shown in green and ancestral wild relatives in gray.

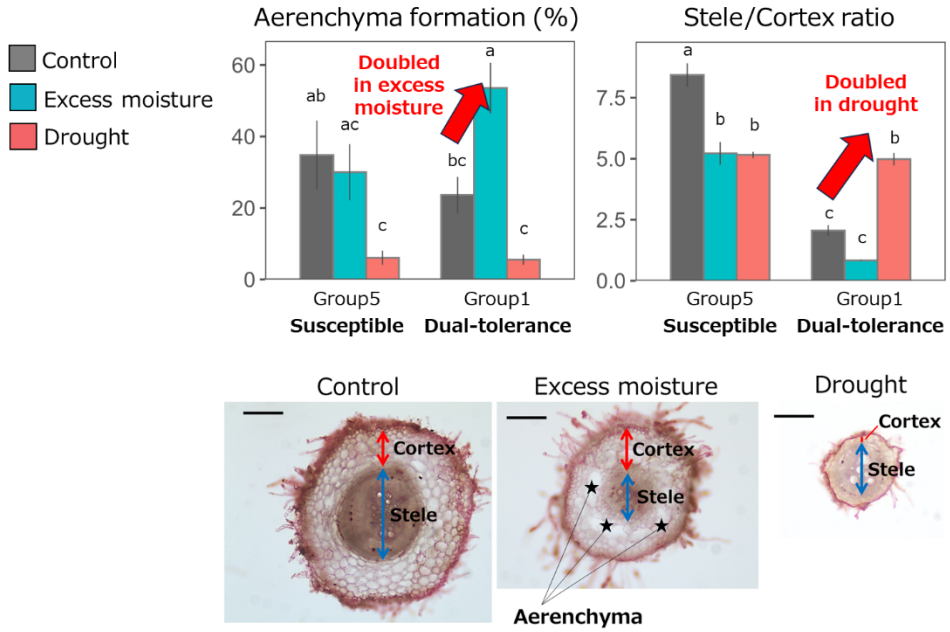

Root morphological changes in an accession of Group1

Fig. 2. Root morphological responses to drought and excess moisture in tolerant (Group 1) and susceptible (Group 5) cowpea

Upper panels show the mean ± SE of aerenchyma formation rate (left) and cortex-to-stele ratio (right). Different letters indicate significant differences at the 5% level (Tukey's test). Lower panels show root cross-sections taken 4–5 cm from the plant base. Red arrows indicate cortex, blue arrows indicate stele, and black stars indicate aerenchyma (scale bar = 200 µm). Tolerant accessions showed increased aerenchyma under excess moisture and a higher stele proportion under drought.

Reference: Iseki and Olaleye (2025) *Frontiers in Plant Science* 16: 1573313. © Author(s) 2025
The figures are reprinted/modified from Iseki and Olaleye (2025) under the terms of the CC-BY 4.0 license.
https://creativecommons.org/licenses/by/4.0/deed.en

A deep learning-based soil diagnostic method for simultaneous multi-parameter analysis using full-wavelength ICP spectra

Rising global food demand and accelerating climate change are intensifying the need for agricultural systems that sustain productivity while conserving limited natural resources. Maintaining healthy soils is central to this challenge, as effective fertilization and management require accurate knowledge of soil properties. However, conventional soil analyses are often costly and time-consuming, limiting their application in many agricultural regions, particularly in developing countries. Consequently, affordable and accessible soil diagnostic technologies are urgently needed. Optical sensing approaches, such as near-infrared (NIR) and mid-infrared (MIR) spectroscopy, have been explored as non-destructive alternatives, but remain limited in the number of soil properties that can be simultaneously assessed.

Here we developed a rapid and low-cost soil diagnostic approach capable of simultaneously estimating multiple soil properties by applying deep learning to the full emission spectrum obtained from an inductively coupled plasma atomic emission spectrometer (ICP-AES).

A total of 1,941 soil samples collected from seven countries, primarily in Africa and Asia, were analyzed using conventional laboratory methods and used as training data. Twelve soil parameters were included: pH (H_2O and KCl), electrical conductivity (EC), available phosphorus (Bray-1), exchangeable Ca, Mg, K, and Na, exchangeable Al, cation exchange capacity (CEC), total carbon, total nitrogen, and particle-size composition (clay and sand contents). In conventional ICP analysis, only selected wavelengths corresponding to target elements are used for quantification. In contrast, this study utilized the entire spectral information. Soil extracts obtained using 1 M ammonium acetate (pH 7) were measured, and intensity values from 2,574 pixels representing 234 wavelength targets were extracted and log-transformed for deep learning input.

The dataset was randomly divided into 80% training and 20% evaluation data, and model training was conducted using a feed-forward neural network (FFNN). Predictive performance was evaluated using the indices proposed by Malley et al. (2004) and Chang et al. (2001). The proposed method predicted all twelve soil parameters with high accuracy: most variables showed coefficients of determination (R^2) greater than 0.9, while even the lowest-performing variable, total carbon, achieved an R^2 of 0.812. Notably, soil properties not directly measurable by ICP, including pH and CEC, were also predicted with high accuracy (Fig. 1), and all parameters reached accuracy levels suitable for practical soil diagnostics (Table 1). This technology reduces costs for reagents, equipment, and time, enabling affordable soil diagnostics (Fig. 2).

Authors: Nakamura, S., Ikazaki, K. [JIRCAS], Imaya, A. [FFPRI]

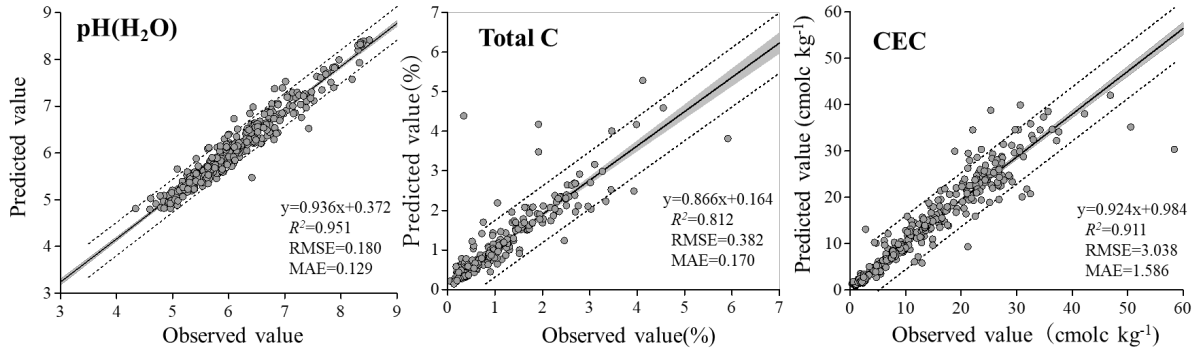

Fig. 1. The relationship between the predicted values and the observed values

RMSE (Root Mean Squared Error) and MAE (Mean Absolute Error)

Table 1. Prediction accuracy for each parameter and its accuracy for soil diagnosis

Parameter	Unit	Determination Coefficient	Results of the Soil Diagnostic Accuracy Assessment	
		R^2	Malley's index	Chang's index
pH (H2O)		0.951	A	A
pH (KCl)		0.959	A	A
EC	mS m^{-1}	0.960	A	A
Bray1-P	mg kg^{-1}	0.963	A	A
Ex. Al	cmolc kg^{-1}	0.964	A	A
Ex. Ca		0.995	A	A
Ex. Mg		0.983	A	A
Ex. K		0.993	A	A
Ex. Na		0.946	B	A
CEC		0.911	B	A
Total N	%	0.956	A	A
Total C		0.812	C	A
Clay		0.844	C	A
Sand		0.870	D	A

Malley et al. 2004
A: Excellent, B: Successful, C: Moderately Successful, D: Moderately Useful, E: Screening

Chang et al. 2001
A: Successful, B: Possibility, C: Not Useful

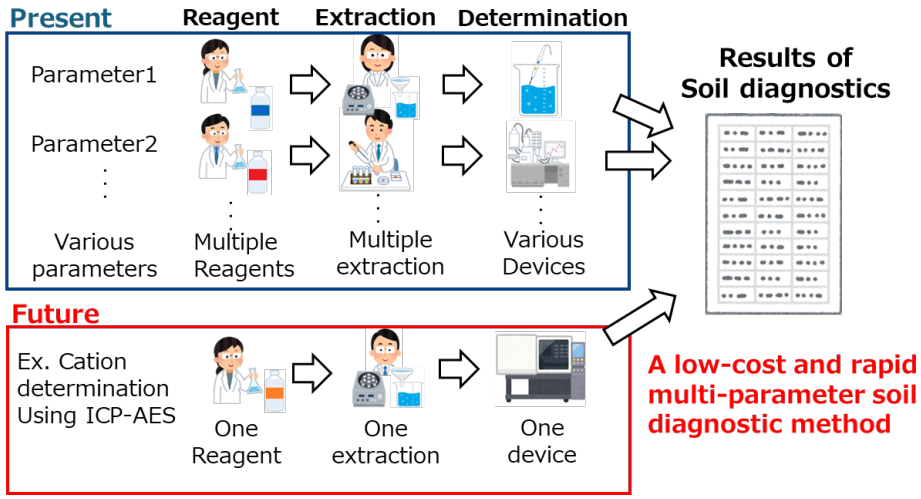

Fig. 2. Present and Future of Soil Diagnosis

Reference: Nakamura et al. (2025) *Scientific Reports* 15: 37753. © Author(s) 2025
The figures are reprinted/adapted from Nakamura et al. (2025) under the terms of the CC-BY 4.0 license.
https://creativecommons.org/licenses/by/4.0/deed.en

Farmers' views on soil fertility: Validity of farmers' perceptions of soil fertility and their application to field management

Soil fertility varies widely across the savanna zone of Sub-Saharan Africa, where smallholder farmers often face financial constraints in purchasing chemical fertilizers. In addition, since conventional soil testing methods remain costly, farmers adopt them only on a limited scale. Under such conditions, efficient allocation of limited resources—e.g., selecting appropriate crops and applying scarce organic amendments—is critical to sustain agricultural productivity. In contrast, farmers have long relied on experiential knowledge to assess soil fertility using observable indicators such as soil color and texture in a way that integrate these perceptions into everyday field management decisions. Understanding the validity and relevance of farmers' soil assessments is therefore essential for promoting sustainable, locally adapted soil fertility management strategies.

This study examines croplands in Northern Ghana in the West African savanna and evaluates the consistency between farmers' perceptions of soil fertility and the measured physicochemical properties of soils. Across 60 rural communities, soil samples were collected from 300 fields, and farmers managing these fields were interviewed regarding their field-level fertility assessments and management practices.

The farmers use soil color, soil texture, and weed species as the main indicators of soil fertility (Fig. 1). They categorize fields into fertile, normal, less fertile, and infertile classes. Perceived higher fertility is significantly associated with higher pH, EC, total C and N, available P, exchangeable bases, and cation exchange capacity—demonstrating strong alignment between farmer perceptions and empirical soil data (Table 1).

Farmers' fertility assessments also shape crop choices (Fig. 2). As the main staple, maize is cultivated across all fertility levels, but cash crops such as groundnut, soybean, and yam are largely excluded from fields perceived as low fertility. Although the overall use of organic inputs remains low (7%), their application shows a distinct pattern (Table 2): farmers preferentially apply organic materials to fields considered either highly or very poorly fertile. This pattern suggests strategic allocation of scarce resources that balance the need for rehabilitating degraded soils with maximizing returns from productive fields.

The results highlight the value of integrating farmers' soil knowledge into agricultural extension and policy planning. Utilizing farmer-based soil assessments can support the development of more context-appropriate recommendations for crop placement, fertilizer strategies, and sustainable soil management. Likewise, the broader adoption of organic amendments requires innovations that address current resource shortages as well as institutional support that improves access to organic inputs.

Authors: Yageta, Y., Koide, J., Muranaka, S., Nakamura S. [JIRCAS], Awuni, A.J., Avornyo, K.J. [UDS]

Table 1. Physicochemical soil properties by farmers' perceptions of soil fertility

	n (total 300)	pH(H2O)		pH(KCl)		EC mS/m		T-N g/kg		T-C g/kg		AP mgP/kg		Ca cmolc/kg		K cmolc/kg		Mg cmolc/kg		Na cmolc/kg
FERTILE	21	**6.90**	**a**	**6.12**	**a**	**11.84**	**a**	**1.08**	**a**	**14.30**	**a**	**115.38**	**a**	**9.21**	**a**	**0.53**	**a**	**1.79**	**a**	0.03
NORMAL	222	6.52	b	5.62	b	5.66	b	0.65	b	8.42	b	15.69	b	4.22	b	0.22	b	1.10	b	0.02
LESS FERTILE	48	6.43	b	5.50	b	4.26	b	0.50	c	6.35	c	9.78	b	2.81	b	0.17	b	0.84	c	0.02
INFERTILE	9	6.04	c	5.33	b	3.96	b	0.39	c	4.12	c	16.65	b	1.86	b	0.19	b	0.49	c	0.01
Average		6.47		5.64		6.43		0.66		8.30		39.38		4.53		0.28		1.06		0.02 n.s.

	n (total 300)	ECEC cmolc/kg		CEC cmolc/kg		Sand %	Silt %	Clay %	
FERTILE	21	**11.72**	**a**	**8.40**	**a**	77.6	11.8	**10.6**	**a**
NORMAL	222	5.69	b	6.00	b	77.8	13.2	9.0	ab
LESS FERTILE	48	3.93	c	4.30	c	80.1	12.7	7.1	c
INFERTILE	9	2.65	bc	2.50	c	82.4	11.7	5.9	bc
Average		6.00		5.30		79.5 n.s.	12.4 n.s.	8.2	

Alphabet letters indicate results of multiple comparisons using the Bonferroni method ($p < 0.05$).

Fig. 1. Soils classified by color and texture

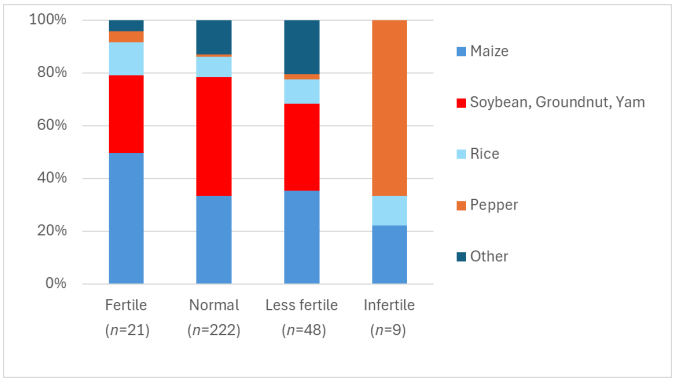

Fig. 2. Crop selection by farmers' perceptions of soil fertility

Table 2. Application rate of organic amendments by farmers' perceptions of soil fertility

		Farmers' Perception of Soil Fertility				Overall field-level application rate
		Fertile (*n*=21)	Normal (*n*=222)	Less fertile (*n*=48)	Infertile (*n*=9)	
Organic Material Application Rate		29%	4%	2%	56%	7%
Application Rate by Type of Organic Material※	Livestock Manure	19%	2%	0%	44%	4%
	Crop Residues	0%	1%	2%	33%	2%
	Compost	10%	1%	0%	11%	2%

※Totals for low-fertility fields do not equal the overall total because some fields overlap across organic amendment categories.

Reference: Yageta et al. (2025) *Geoderma Regional* 41: e00972. © Authors 2025
The figures are reprinted/modified from Yageta et al. (2025) under the terms of the CC-BY 4.0 license.
https://creativecommons.org/licenses/by/4.0/deed.en

Socio-structural factors in the adoption and farmer-to-farmer dissemination of soil conservation technologies

In Burkina Faso, erratic rainfall and overcultivation cause severe soil degradation. Although farmers use traditional conservation technologies like Zaï (Fig. 1A), stone lines (Fig. 1B), and organic manure (Fig. 1C), their widespread adoption remains limited. A primary barrier is the chronic shortage of public extension workers. While farmer-to-farmer extension—sharing technologies among peers—is a promising supplement, empirical knowledge regarding the conditions for its success and dissemination pathways remains insufficient. This study aims to comprehensively understand farmer-to-farmer extension and quantitatively assess how socio-structural factors and technology-specific traits impact dissemination.

The results reveal that Zaï adoption correlates positively with larger landholdings and higher proportions of native residents, whereas religious homophily acts as a constraining factor (Table 1A). Its dissemination is driven by native and highly educated farmers (Table 1D), highlighting the role of resources and local connections. In the case of labor-intensive stone lines are adopted mostly by male-headed households (Table 1B) and disseminate effectively in villages with strong religious homophily (Table 1E), suggesting that social cohesion supports the necessary collaborative labor. Finally. As for organic manure, adoption increases with the proportion of native residents (Table 1C), but its dissemination shows no statistically significant differences across social groups (Table 1F). Furthermore, risk aversion—measured via behavioral games—shows no correlation with technology adoption or dissemination (Table 1). This indicates that social constraints and role divisions, rather than individual risk preferences, primarily drive adoption.

These findings support the development of practical extension models that complement public systems in resource-constrained regions. By leveraging the identified social conditions, extension strategies can be customized based on local trust networks. Specifically, highly educated and native residents can serve as effective hubs for Zaï, whereas cohesive religious communities are ideal for spreading stone lines. Given the tendency for male-headed households to adopt labor-intensive practices, introducing support packages tailored to specific technology characteristics ensures that female farmers are not excluded. This approach helps establish sustainable dissemination models applicable beyond Burkina Faso. Finally, since environmental factors like precipitation were not fully examined, future research should integrate both social and natural conditions for comprehensive extension designs.

Authors: Lee, G., Ikazaki, K., Muraoka, R. [JIRCAS], Sawadogo-Compaoré, E., [INERA]

（A）Zaï （B）Stone lines （C）Organic manure

Fig. 1. Examples of Zaï, stone lines, and organic manure practices

This figure illustrates three widely used soil conservation technologies in Burkina Faso: Zaï, stone lines, and organic manure. Zaï is a rainwater harvesting and storage technique using planting pits. Stone lines involve arranging stones in rows to mitigate soil erosion. Organic manure is applied to

Table 1. Determinants of adoption and farmer-to-farmer dissemination of soil conservation technologies

	Adoption			Farmer-to-farmer dissemination		
	A. Zaï	B. Stone	C. Organic	D. Zaï	E. Stone	F. Organic
Household attributes						
Male head	0.02	0.25***	0.04	-0.04	-0.06	-0.02
	(0.04)	(0.08)	(0.06)	(0.06)	(0.04)	(0.03)
Native head	-0.06	-0.09	-0.06	0.12*	0.04	0.03
	(0.05)	(0.05)	(0.04)	(0.06)	(0.06)	(0.03)
Head's education	-0.01	0.01	-0.002	0.04**	0.02	0.01
	(0.02)	(0.02)	(0.02)	(0.02)	(0.01)	(0.01)
Head's risk aversion	0.002	0.01	-0.001	-0.01	-0.001	-0.0004
	(0.01)	(0.01)	(0.01)	(0.01)	(0.004)	(0.003)
Farm land area（log）	0.08**	0.06	0.01	0.01	-0.01	-0.01
	(0.04)	(0.04)	(0.03)	(0.05)	(0.05)	(0.02)
Village attributes						
Native household ratio	0.77**	-0.29	0.77**	-0.14	0.16	0.10
	(0.26)	(0.38)	(0.32)	(0.42)	(0.35)	(0.15)
Religious homophily	-0.72***	-0.34	-0.18	0.17	1.40***	0.01
	(0.26)	(0.27)	(0.20)	(0.28)	(0.46)	(0.14)
District fixed effects	YES	YES	YES	YES	YES	YES
Pseudo R^2	0.02	0.04	0.08	0.18	0.002	0.08
Sample size	650	650	650	227	195	466

"Stone" and "Organic" stand for stone lines and organic manure, respectively. Columns (1)–(3) display the estimation results using the adoption of each technology as the dependent variable for the entire sample of 650 households. In contrast, Columns (4)–(6) include only the households that have already adopted the corresponding technology, with the occurrence of farmer-to-farmer dissemination as the dependent variable. The values presented are the marginal effects from the logit models (representing the change in the probability of adoption or dissemination). As each

Reference: Lee et al. (2026) *Land Degradation & Development,* 37: 704–719. © The Author(s) 2026
The figures are reprinted/modified from Lee et al. (2026).
https://creativecommons.org/licenses/by/4.0/deed.en

Selective application of farmyard manure improves rice yields in phosphorus-deficit paddies in Sub-Saharan Africa

Rice demand in Sub-Saharan Africa is increasing rapidly, yet rice productivity remains low, averaging only 2.3 t ha^{-1}. Smallholder farmers in the region often cultivate rice under severe soil fertility constraints, particularly in strongly weathered soils where phosphorus (P) deficiency is common. Although mineral fertilizers can increase yields, their high cost and limited accessibility often restrict their use. Under such conditions, farmyard manure (FYM), which can be produced locally from livestock manure and plant residues, represents an important on-farm resource. Previous studies have suggested that organic amendments such as FYM can improve P availability by mobilizing soil-bound P, but evidence from farmers' fields showing how FYM effectiveness varies with soil P status has remained limited.

To address this gap, field experiments were conducted for four consecutive cropping seasons in four farmers' rice paddies in the central highlands of Madagascar that differed in available soil P. FYM was applied annually at 10 t ha^{-1} (fresh weight), corresponding to the level commonly used by local farmers. Yield responses to FYM were substantially greater in P-deficit paddies than in non-deficit paddies. Over four seasons, the average yield gain with FYM reached 1.5 t ha^{-1} in P-deficit paddies, compared with only 0.4 t ha^{-1} in non-deficit paddies (Fig. 1). The cumulative effect of repeated FYM application also became larger over time, and the greatest response was observed when FYM was combined with nitrogen (N) fertilizer, with yield gains of up to 3.1 t ha^{-1}. In P-deficit paddies, the average yield gain achieved with FYM alone corresponded to 77% of that obtained with inorganic N and P fertilizer (Fig. 2). In addition, a synthesis of 13 field trials from six countries in Sub-Saharan Africa showed the same general pattern, confirming that FYM application is consistently more effective under P-deficit conditions (Fig. 3).

These results demonstrate that the agronomic effectiveness of FYM depends strongly on soil P status and that P-deficit paddies should be prioritized when FYM resources are limited. The findings provide a scientific basis for the selective use of FYM in rice systems of Sub-Saharan Africa. By targeting FYM to fields where it is most effective, farmers can make more efficient use of locally available organic resources, improve rice productivity, and reduce reliance on costly mineral fertilizers.

Asai, H., Tsujimoto, Y., Nishigaki, T. [JIRCAS], Andriamananjara, A., Rakotonindrina, H. [LRI]

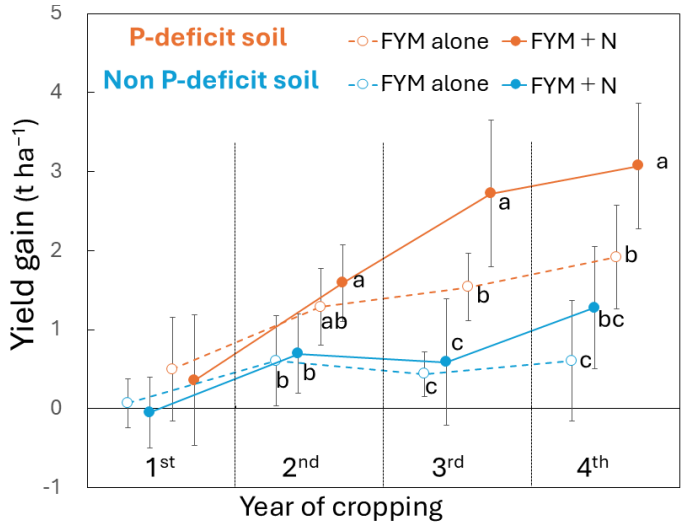

Fig. 1. Yield response to repeated application of farmyard manure (FYM)

Means of two P-deficit and two non-P-deficit paddies. P-deficit soils were defined as Bray-II P ≤ 12 mg P kg^{-1} (Dobermann, 2000). Yield increase was calculated relative to the no-fertilizer control. FYM consisted of cattle manure, plant residues, and rice straw. Nitrogen fertilizer was applied as urea at 80 kg N ha^{-1}. Different letters indicate significant differences (Tukey's test, $p < 0.05$).

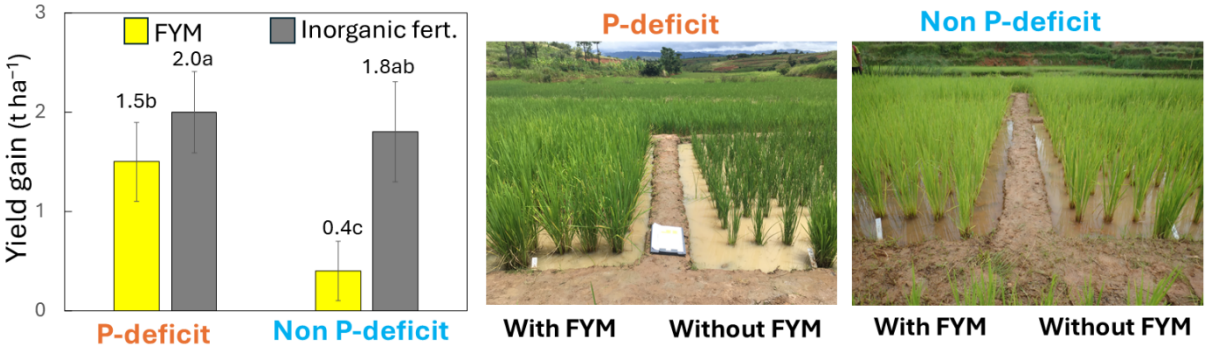

Fig. 2. Yield increase with farmyard manure (FYM) and mineral fertilizer

Mean yield increase over four cropping seasons in two P-deficit and two non-P-deficit paddies, relative to the no-fertilizer control. Mineral fertilizer was applied at 80 kg N ha^{-1} and 50 kg P_2O_5 ha^{-1} each season. The photo (right) compares plant growth at 70 days after transplanting under no-mineral-fertilizer conditions, with and without FYM. Error bars indicate standard deviations. Different letters indicate significant differences (Tukey's test, $p < 0.05$).

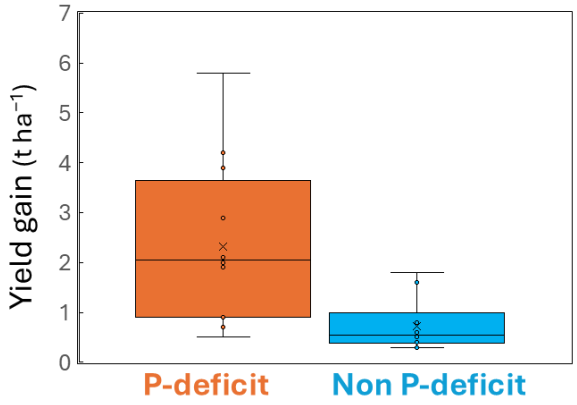

Fig. 3. Yield increase with farmyard manure (FYM) in Sub-Saharan Africa

Yield increase in 13 field trials (eight P-deficit and five non-P-deficit paddies) conducted without mineral fertilizer. Yield increase was calculated as the yield difference between FYM-applied and no-FYM plots. Paddies were classified by available soil P following Dobermann (2000). FYM materials, composition, and application rates differed among trials. The difference between groups was significant (*t*-test, $p < 0.01$).

Reference: Asai et al. (2025) *Field Crops Research* 23: 590 – 601. © Elsevier 2025
The figures are reprinted/modified from Asai et al. (2025) with permission.

Improved tolerance to iron toxicity in rice by knock-down of a citrate transporter FRDL1

Iron (Fe) toxicity is a nutrient disorder that specifically affects lowland rice, limiting its productivity in many regions such as Sub-Saharan Africa and Southeast Asia, typically resulting in yield losses of more than 10%. Despite its significance, our understanding of the genes and mechanisms to enhance Fe toxicity tolerance is limited, and breeding efforts have seen little success. Therefore, further investigation is needed to identify genes that can be used for tolerance breeding. In this study, the author focused on the fact that Fe within roots is transported to the shoot in the form of a citrate-Fe complex, and investigated the effects of mutating citrate transporters on Fe toxicity tolerance.

Wild-type plants, along with loss-of-function mutants for FRDL1 (a transporter that releases citrate in the xylem) and FRDL4 (a transporter that releases citrate to the rhizosphere) were evaluated in a hydroponic system with varying amounts and forms of Fe. Tolerance levels and the mechanisms were examined by measuring foliar symptoms and tissue Fe concentrations. The results showed that the *frdl1* mutant, but not the *frdl4* mutant, exhibited increased tolerance to Fe toxicity (Fig. 1). This suggests that xylem citrate plays a crucial role in determining Fe toxicity tolerance in rice plants, while citrate released in the rhizosphere is less important, at least in the hydroponic system. The *frdl1* mutant exhibited significantly lower Fe concentrations in leaf blades under excess ferrous iron (Fe^{2+}) conditions compared to wild-type plants, while root concentrations remained unaffected (Fig. 2). Contrary to the observation under excess Fe^{2+} conditions, reductions in leaf blade Fe concentrations were not observed under excess chelated Fe (Fe-EDTA) conditions. This suggests that the FRDL1 mutation alleviates Fe toxicity stress only when excess Fe is provided in the form of unchelated Fe^{2+}. To assess if the *frdl1* mutation could enhance tolerance in a sensitive variety, the *frdl1* mutant (Nipponbare background) was crossed with a sensitive *indica* variety, Ciherang, and the resulting F_2 population was evaluated under excess Fe^{2+} conditions. Individuals with the functional Ciherang-type FRDL1 exhibited severe symptoms with high leaf Fe concentrations, while those with the non-functional, mutated FRDL1 showed milder stress symptoms and significantly lower leaf Fe concentrations (Fig. 3).

These results suggest that a malfunctioning of FRDL1 leads to decreased xylem citrate concentrations, resulting in less efficient root-to-shoot Fe translocation (Fig. 4). This indicates that FRDL1 is a promising target to reduce leaf Fe concentration under Fe toxicity conditions. Further research is necessary to understand the factors that regulate the expression of *FRDL1* in roots and apply this knowledge to practical breeding efforts.

Author: Ueda, Y. [JIRCAS]

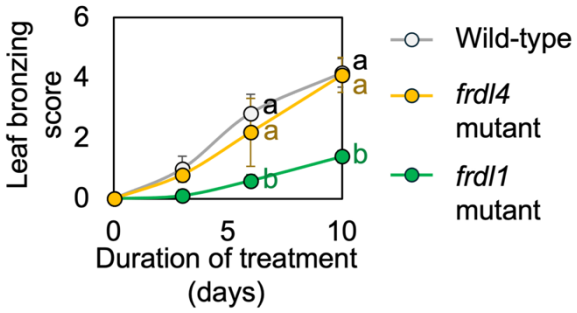

Fig. 1. Formation of leaf symptoms in different genotypes

The degree of leaf symptoms under excess ferrous iron (Fe^{2+}) conditions was quantified by "leaf bronzing score." Higher values indicate more severe symptom formation. Different alphabets indicate significant differences (p<0.05).

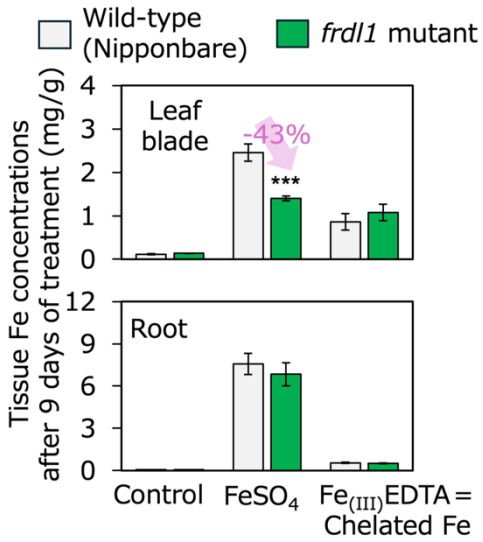

Fig. 2. Tissue Fe concentrations under different treatments

Fe concentrations in leaf blades and roots were measured under the control, excess ferrous iron ($FeSO_4$), and excess chelated iron (Fe-EDTA) conditions. Asterisks (***) indicate that the concentration was significantly different between the wild-type and frdl1 mutant at p<0.001 level.

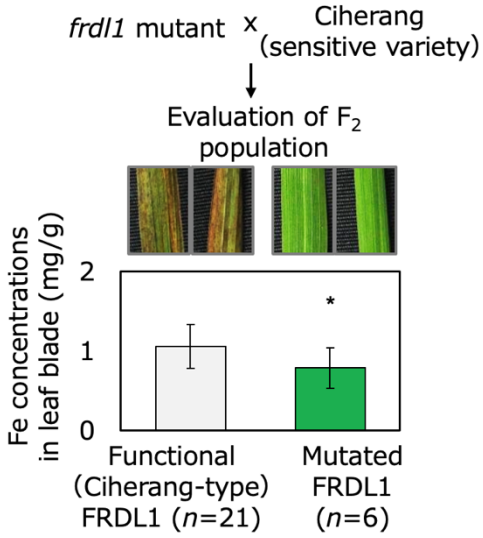

Fig. 3. Effects of FRDL1 mutation in the sensitive Ciherang background

Leaf traits and leaf blade Fe concentrations were evaluated in the F_2 population. Leaves of representative plants are shown. The asterisk (*) indicates that Fe concentrations are significantly different between plants with the functional FRDL1 and mutated FRDL1 at p<0.05 level.

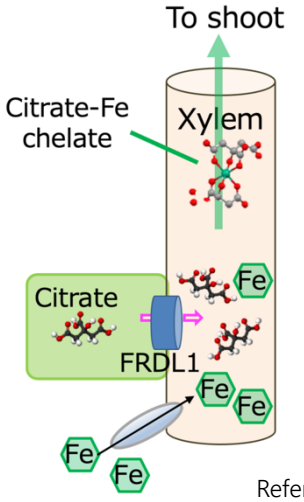

Fig. 4. Possible mechanism for the mitigation effect of Fe toxicity stress in the FRDL1 knock-down line

FRDL1 plays a crucial role for exuding citrate to the xylem. Xylem contains Fe absorbed by plants, and chelation by citrate leads to more efficient translocation of Fe to the shoot. FRDL1 knock-down decreases xylem citrate concentrations, and the concomitant decrease in chelated Fe leads to reduced Fe translocation to the shoot. Chelated Fe (Fe-EDTA) can be transported to the shoot without citrate, and the effects of FRDL1 mutation is not evident.

Reference: Ueda, Y. (2025) *Plant Biology*, https://doi.org/10.1111/plb.70107. © Author 2025
The figures are reprinted/modified from Ueda (2025) under the terms of the CC-BY 4.0 license.
https://creativecommons.org/licenses/by/4.0/deed.en

Soil organic carbon content in paddy soils of the central highlands of Madagascar is regulated by soil geochemistry

Understanding the mechanisms of soil organic carbon (SOC) stabilization is crucial for climate change mitigation. While acid-oxalate-extractable aluminum (active Al) and iron (active Fe) drive SOC stabilization in tropical upland soils, their roles in paddy soils remain poorly understood due to the complex redox dynamics from seasonal flooding and drainage. Furthermore, empirical data on SOC stabilization in sub-Saharan African paddy soils are notably scarce. To address this, this study utilized structural equation modeling to analyze 306 paddy fields across the central highlands of Madagascar. Encompassing diverse parent materials, from volcanic to non-volcanic soils, this first-of-its-kind large-scale comparative research aimed to elucidate the geochemical factors regulating SOC stability in tropical paddy soils.

The analysis revealed that SOC content (0.3% to 13.4%) correlated much more strongly with total active Al and Fe contents than with total clay and silt contents (Fig. 1). Structural equation modeling demonstrated that in Al-dominant soils (primarily volcanic), only active Al contributed to SOC stabilization, whereas in Fe-dominant soils (primarily non-volcanic), both active Al and active Fe played significant roles (Fig. 2). This finding provides the first empirical evidence that the relative balance of active Al and Fe primarily determines SOC stabilization in tropical paddy soils. Additionally, a consistent negative correlation was found between SOC content and soil pH across all soil types, indicating that elevated pH decreases SOC storage in these environments.

These findings highlight the importance of geochemical factors—such as volcanic influence, soil pH, and the ratios of active Al and Fe—in improving the prediction accuracy of carbon sequestration potential in similar tropical paddy ecosystems. Crucially, because raising soil pH through artificial amendments may inadvertently reduce SOC, these results emphasize the need to integrate organic matter inputs when neutralizing acidic tropical soils to balance pH correction with effective SOC storage. While these insights apply to regions sharing similar conditions with the central highlands of Madagascar, further verification is essential before applying them to paddy environments with extended flooding periods, such as triple-cropping systems or floodplains where soil properties are frequently altered by sediment deposition.

Authors: Nishigaki, T., Tsujimoto, Y., Okamoto, T., Oo, A.Z. [JIRCAS],
Lyu, H. [Tokyo Univ. of Agriculture and Technology],
Rakotonindrina, H., Andriamananjara, A., Razafimbelo, T. [LRI], Rakotoarisoa, N.M. [FOFIFA]

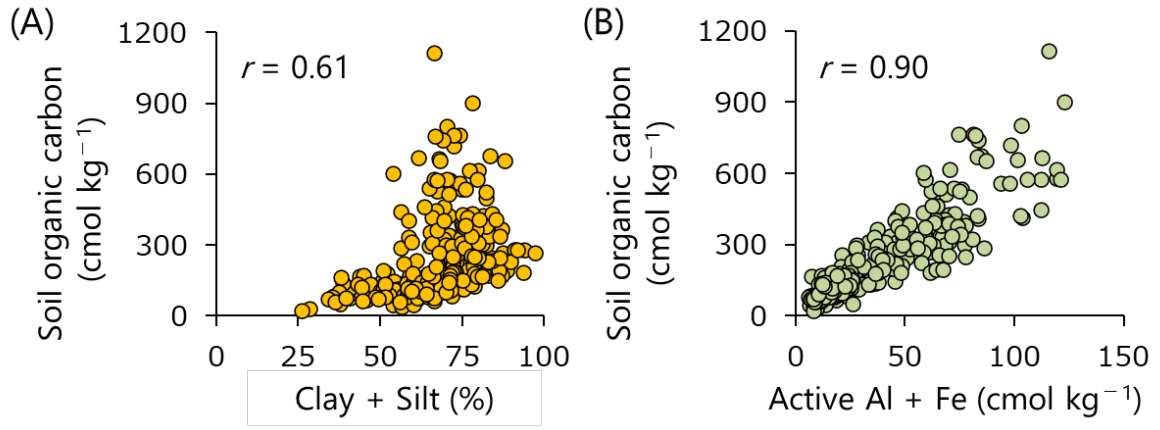

Fig. 1. Relationships between soil organic carbon (SOC) content and (A) clay + silt content, and (B) active Al + active Fe content

The '*r*' in the figures indicates the correlation coefficient. The unit of soil organic carbon content (cmol kg^{-1}) can be converted to % by multiplying it by 12.01 / 1,000.

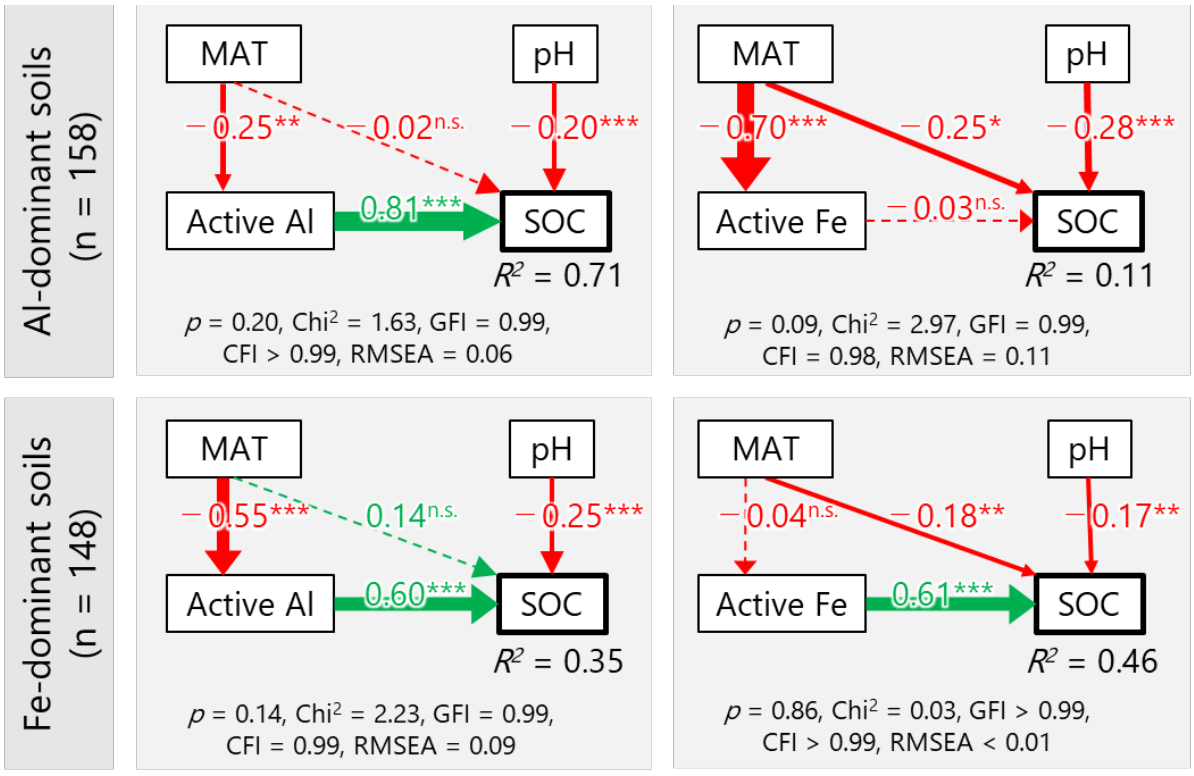

Fig. 2. Structural equation models for variations in soil organic carbon (SOC) content in Al-dominant soils (top) and Fe-dominant soils (bottom)

Red/green arrows indicate negative/positive effects. Numbers on arrows are standardized path coefficients (*** $p < 0.001$, ** $p < 0.01$, * $p < 0.05$, n.s.: not significant). Solid/dashed arrows represent significant/non-significant effects, with thickness reflecting correlation strength. R^2 indicates the explained variance of SOC. Model fit indices: p, Chi^2, GFI, CFI, and RMSEA. MAT: Mean Annual Temperature

Reference: Nishigaki et al. (2025) *Environmental Research* 284: 122277. © 2025 Elsevier Inc.
The figures are reprinted/modified from Nishigaki et al. (2025) with permission.

Technical guidelines for improving water use efficiency in irrigation areas in Africa

In Sub-Saharan Africa, rice consumption has consistently outpaced domestic production, leading to a critical reliance on imports. Therefore, it is essential to increase productivity within irrigation schemes. However, there are some cases where the actual irrigated area falls short of the planned command area due to the functional deterioration of water facilities and inefficient water management. These guidelines were developed to expand technical options by proposing new countermeasures that contribute to efficient water utilization.

In the Lower Moshi area, leakage in earth canals was measured at 43 mm h^{-1} after the commencement of farming (Fig. 1). By implementing countermeasures to mitigate leakage (Fig. 2C, D), water loss is reduced, enabling the supply of additional water to downstream areas. Furthermore, concrete canal surfaces become increasingly rough over time, impairing water flow. A resin-based coating method (Fig. 2B) can significantly improve water flow by 36% to 46% (Fig. 3). In the same cross section as that used in the field trial, this resulted in a flow rate increase of 56% to 84% (at a water depth of 0.6 m). Implementing plot leakage countermeasures—such as towing a Cambridge roller (Fig. 2E) and removing the topsoil to directly compact the hardpan—resulted in a 5 mm reduction in water requirement per day (WRPD) (Fig. 4). These guidelines describe several other methods to increase the irrigated area through efficient water utilization, including: upgrading diversion works, improving field drainage using cut drains, powering pump irrigation with small-scale hydropower using the flow within irrigation canals, installing recirculation subsurface irrigation powered by solar energy (Fig. 2F–I), adopting water-saving cultivation via the alternate wetting and drying (AWD) method, and implementing appropriate water allocation to improve water use efficiency (Fig. 5).

By applying these technologies to the 2019 conditions of the Lower Moshi District, there is potential to expand the irrigated area to 2,273 ha (152% of the original planned command area of 1,500 ha) (Fig. 6). These guidelines are available in English, Japanese, and Swahili on the JIRCAS website.

Successful implementation requires addressing financial and social factors. Since many of these technologies involve initial costs, the development of agricultural credit systems is recommended. While these methods are designed for broad application by farmers and engineers, pilot testing is advised to adapt them to local soil and climatic conditions. Crucially, as these improvements benefit the entire irrigation block rather than just individual plots, fostering community consensus and collective agreement among water users is vital for the sustainable management of improved water resources.

Authors: Hirouchi, S., Onishi, J., Yamada, M., Shindo, S., Furihata, H., Ishijima, M., Uno, K., Yanagihara, S., Hirose, C., Uchimura, M., Yokoyama, S. [JIRCAS]

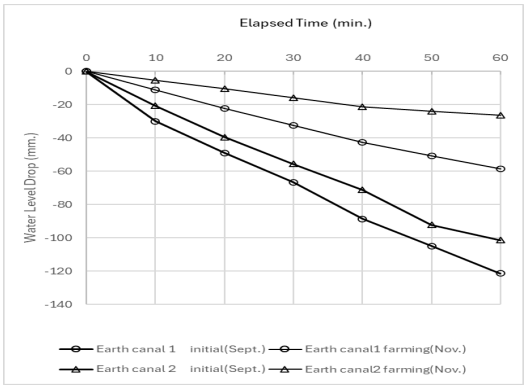

Fig. 1. Results of earth canal infiltration test

Infiltration rate from earth canals (Lower Moshi area): Average 111.5 mm h^{-1} before and 43 mm h^{-1} after the start of farming

Fig. 2. Measures described in the guidelines

Resin coating (A: before, B: after), earth canal leakage measures (C: polyethylene sheet, D: PVC pipe), E: plot leakage measure, F: sub-surface irrigation, G: shallow sub-surface drainage, H: small hydropower, I: division box renewal

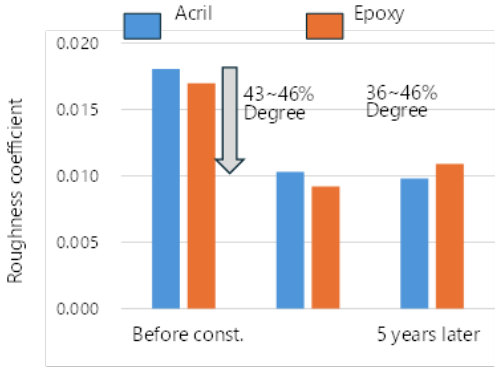

Fig. 3. Effect of surface coating

Epoxy- and acrylic-resin-coated concrete canals resulted in a 43–46% reduction in roughness half a year after application, and a 36–46% reduction after five years.

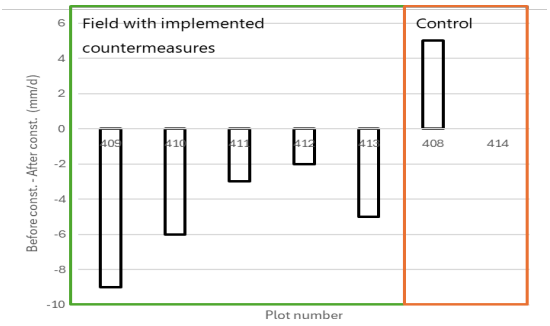

Fig. 4. WRPD in plots treated with the crushing and compaction method

Average WRPD of the plots where the crush and compaction method were implemented (Plots 409–413) decreased by 5.0 mm (29%).

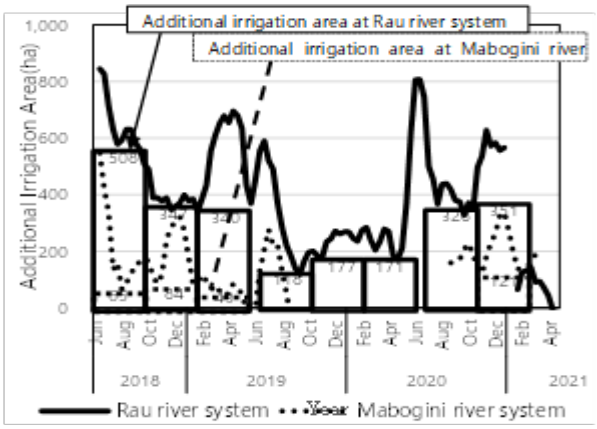

Fig. 5. Additional irrigable area

Calculated by subtracting the required irrigation volume from the monthly irrigation water volume by river system

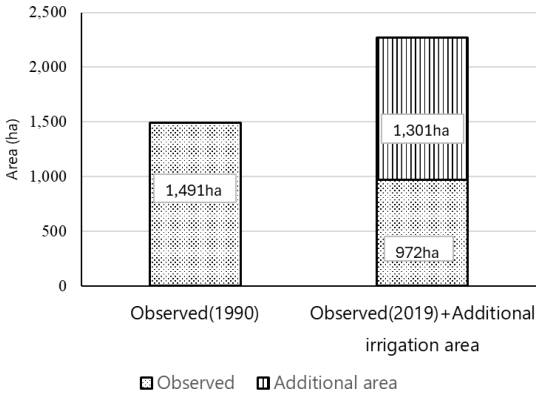

Fig. 6. Potential additional irrigation area by measure implementation

Actual irrigated area: 1,491 ha (in 1990), 972 ha (in 2019). Estimated expandable area: 1,301 ha

The figures are reprinted/modified from Hirouchi et al. (2022) (Fig. 1) ©JSIDR with permission; Hirouchi et al. (2025a) (Fig. 2) ©Authors 2025 under the terms of the CC-BY 4.0 license (https://creativecommons.org/licenses/by/4.0/deed.en); and Hirouchi et al. (2025b) (Figs. 3–5) ©JSIDR with permission.

A simple photosynthesis measurement device using a compact, low-cost microcomputer and CO_2 sensor

Leaf photosynthetic rate is a growth assessment indicator used in many contexts within the field of plant science. The assimilation chamber method is one of its measurement techniques, and commercially available portable measuring devices were first introduced approximately 40 years ago. Today, their successor models are the mainstream choice due to advantages such as superior measurement accuracy and speed. On the other hand, the high cost (ranging from several million to over 10 million yen, and subject to further increases due to social conditions and exchange rate fluctuations) is the primary concern preventing a wide range of users (researchers, producers, educators, etc.) from utilizing photosynthesis measurement devices.

We developed a prototype closed-system photosynthesis measurement system (hereinafter referred to as the "demo device") that incorporates an inexpensive CO_2 sensor into a custom-built assimilation chamber and is controlled and recorded by a small microcomputer (Fig. 1a,b). The demo device can be built inexpensively with material costs of approximately 30,000 yen. When the measurement performance of the demo device was compared to that of a standard unit using sugarcane leaves, a significant correlation between the measured values was observed in both cases: when light intensity was varied using artificial light sources in a temperature- and humidity-controlled room (Fig. 2a) and when multiple varieties were measured under natural outdoor light conditions (Fig. 2b). The accuracy of a simple linear regression model using the photosynthesis rate measurements from these devices was sufficiently high with low values of root mean square error under all conditions, highlighting the high measurement accuracy of the demo device.

Our results indicate that as photosynthesis measurements become more affordable and accessible, photosynthesis research will become more accessible to many researchers with limited budgets, thereby stimulating research in related fields. These results do not guarantee performance equivalent to that of the standard unit; it is recommended that the demo device and the standard unit be used for different purposes as appropriate. Since inexpensive CO_2 sensors may vary in performance and durability, it is necessary to verify their performance under atmospheric CO_2 conditions or known CO_2 concentrations as appropriate. To apply this system to the evaluation of multiple samples (high-throughput phenotyping), such as genetic resources or hybrid populations, improvements to the data recording system (e.g., from wired to wireless) and the measurement system (e.g., from closed to open) should be considered.

Authors: Takaragawa, H. [JIRCAS], Asahi, T., Mitsuoka, M., Taira, E., Kawamitsu, Y. [Univ. of the Ryukyus]

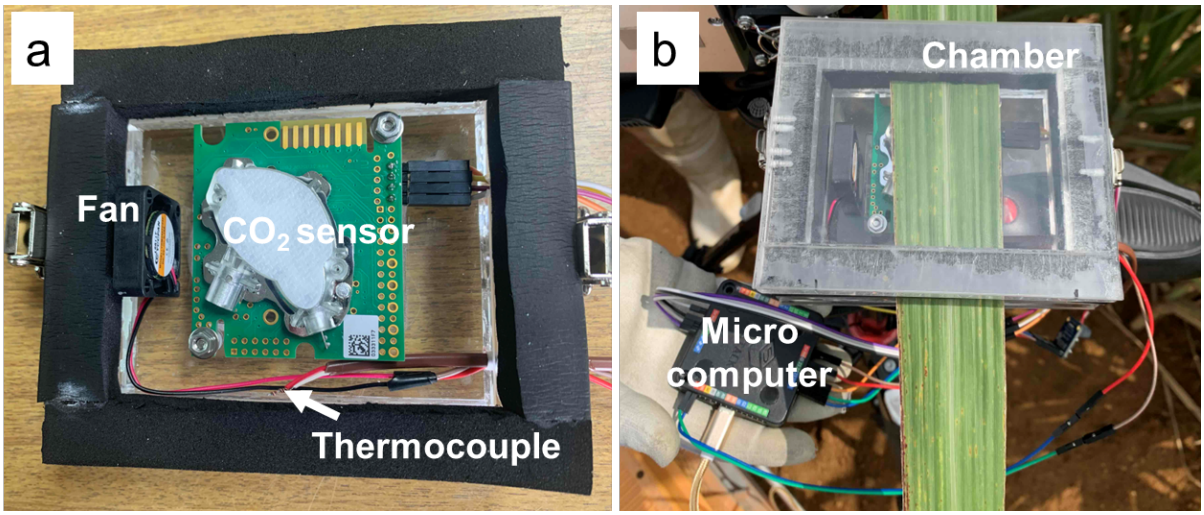

Fig. 1. Outline of demo device

The sensors inside the assimilation chamber (a) and the demo device during measurement (b) are shown. A CO_2 sensor, fan, and thermocouple are installed inside the assimilation chamber, and these are connected to an external microcontroller via jumper wires to drive them.

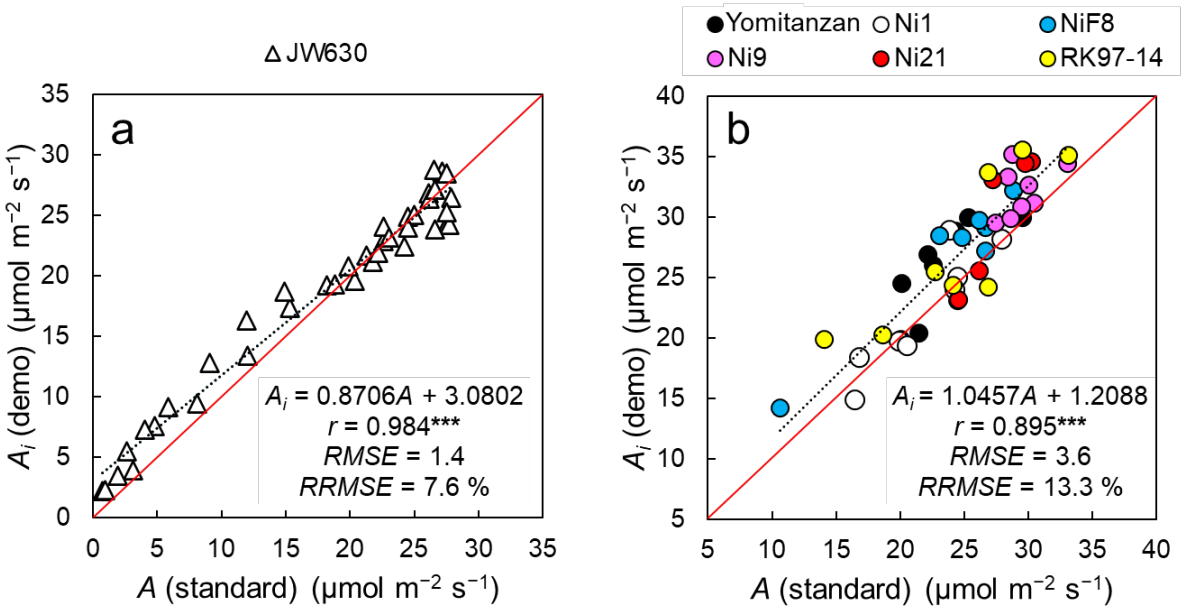

Fig. 2. Comparison of photosynthetic rates in sugarcane leaves measured using the demo device and a standard unit

A_i (demo device) and A (standard unit) represent the photosynthetic rates measured using the demo device and standard unit (with light-transmitting chamber), respectively (a: data obtained by varying light intensity using a single line in a temperature- and humidity-controlled glasshouse (n=50); b: data obtained using multiple varieties in a field environment (n=45)). The dashed lines represent the linear regression equations with A_i as the dependent variable and A as the independent variable. r denotes the correlation coefficient, and *** indicates that the correlation is significant at the 0.1% level. RMSE and RRMSE denote the root mean square error and relative root mean square error, respectively; lower values indicate higher accuracy of the regression equation. The solid red line represents y = x.

Reference: Takaragawa et al. (2025) *Photosynthesis Research* 163: 52. © Authors 2025

The figures are modified from Takaragawa et al. (2025).

Intergeneric hybrid between sugarcane and *Erianthus* exhibits superior leaf water-use efficiency compared to sugarcane

Erianthus arundinaceus, a closely related genus to sugarcane (*Saccharum* spp.), is expected to contribute to improving sugarcane's drought tolerance through interspecific hybridization. So far, JIRCAS has reported *Erianthus* traits associated with drought tolerance, including excellent root system development, leaf gas exchange characteristics (water use efficiency; WUE—calculated by dividing photosynthetic rate by stomatal conductance, a measure of transpiration), and metabolite adaptations. While reports exist on the root system development of intergeneric hybrids between sugarcane and *Erianthus*, there are no reports on the leaf characteristics (gas exchange and morphological traits) of their hybrids, and the potential for improving sugarcane leaf characteristics through intergeneric hybridization remains unclear.

We investigated the leaf gas exchange characteristics, morphological traits, and dry matter allocation patterns of a sugarcane variety (NiF8), an *Erianthus* accession (JW630), and an intergeneric F_1 hybrid (J16-77 [NiF8 x JW630]) derived from these parents under pot conditions at JIRCAS-TARF, to verify the potential for improving these traits through intergeneric hybridization. Although the difference was not significant under high-light conditions, *Erianthus* showed higher WUE than that of sugarcane regardless of soil moisture conditions (Fig. 1). Genotypic differences in WUE became more pronounced under low-light conditions (photosynthetic photon flux density of 500 μmol m^{-2} s^{-1}) compared to high-light conditions (2,000 μmol m^{-2} s^{-1}) during gas exchange measurements (Fig. 1). Compared to sugarcane, *Erianthus* has a lower stomatal density on the abaxial side of the leaves, a higher ratio of adaxial to abaxial stomatal density, and longer interveinal distances (Table 1). These differences are largely due to genetic factors. Sugarcane allocates a large proportion of dry matter to the stem, whereas *Erianthus* allocates more to the leaves and roots (Fig. 2). The WUE and stomatal density of the F_1 hybrid are comparable or close to those of the *Erianthus* parent (Fig. 1, Table 1). On the other hand, the F_1 hybrid shows a large proportion of dry matter allocation to the stem similar to that of the sugarcane parent (Fig. 2).

Through intergeneric hybridization, it is possible to develop hybrids that inherit leaf characteristics from the *Erianthus* parent and dry matter allocation to the stem from the sugarcane parent, thereby combining the characteristics of both parents. The F_1 hybrid possesses desirable above-ground traits which may contribute to improving sugarcane drought tolerance, although further field studies will be required. Because the tested F_1 hybrid has low sugar content at harvest, improving sugar content through backcrossing with sugarcane varieties is necessary for their utilization as breeding materials.

Authors: Takaragawa, H., Terajima, Y., Okamoto, K. [JIRCAS]

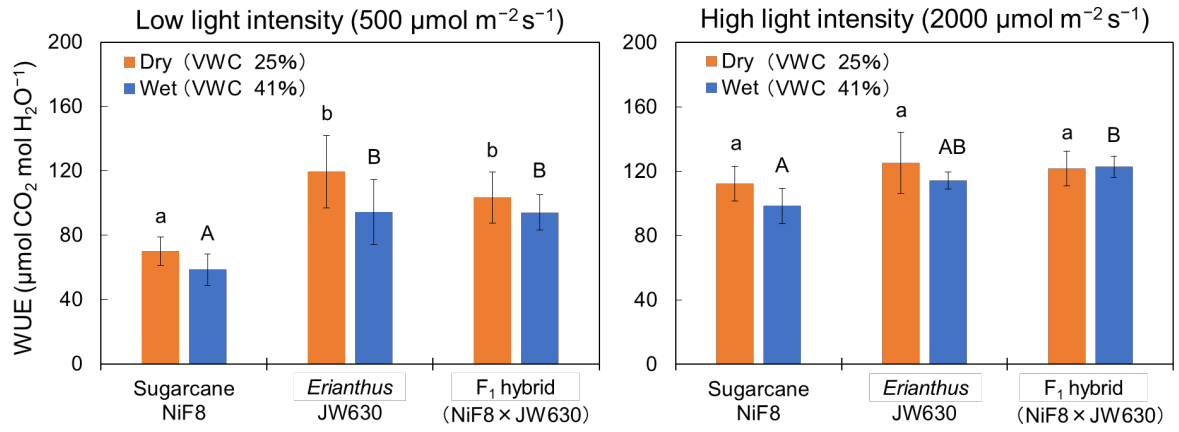

Fig. 1. Effects of soil moisture and light intensity on water use efficiency (WUE) in sugarcane, *Erianthus*, and intergeneric F_1 hybrid

The results measured on Sep. 26, 2021, during the soil drying treatment, under low-light (photosynthetic photon flux density 500 μmol m^{-2} s^{-1}; left panel) and high-light (2,000 μmol m^{-2} s^{-1}; right panel) conditions are shown. The orange and blue bars represent data from the dry (soil volumetric water content; VWC 25%) and the wet (41%) treatments, respectively. Error bars indicate standard deviation (n = 4). Different letters indicate differences among treatment groups within the same light intensity × soil moisture condition (Tukey's test, $p < 0.05$, n = 4).

Table. 1. Leaf morphological characteristics in sugarcane, *Erianthus*, and intergeneric F_1 Hybrid

Treatment	Genotype	Stomatal density (no. mm^{-2})			Interveinal distance (μm)
		Adaxial	Abaxial	Ad/Ab	
Wet	Sugarcane NiF8	93 a	178 b	0.52 a	123 a
	Erianthus JW630	98 a	135 a	0.73 c	140 b
	F_1 hybrid (NiF8 x JW630)	99 a	148 a	0.67 b	152 b
Dry	Sugarcane NiF8	94 A	177 C	0.53 A	129 A
	Erianthus JW630	100 AB	138 A	0.72 B	147 B
	F_1 hybrid (NiF8 x JW630)	106 B	160 B	0.66 B	154 B

Different letters indicate significant differences between genotypes within each treatment (Tukey's test, $p < 0.05$, n = 4).

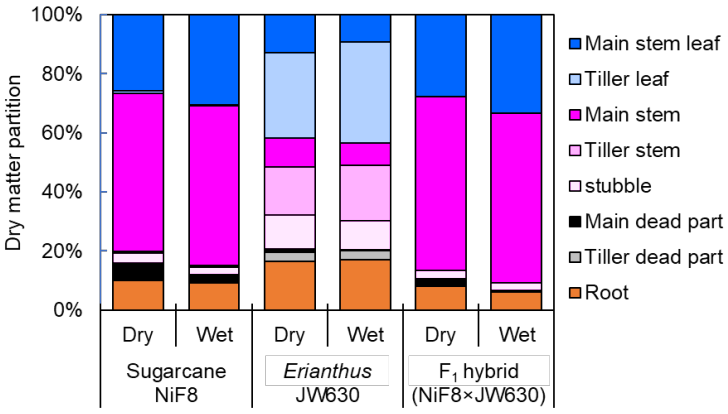

Fig. 2. Biomass partition in sugarcane, *Erianthus*, and intergeneric F_1 hybrid

The dry matter partition indicates the percentage of dry matter in each plant part relative to the total dry matter weight. Sugarcane and intergeneric hybrid exhibit similar dry matter allocation characteristics, such as a high dry matter allocation ratio to the stem.

Reference: Takaragawa et al. (2025) *Frontiers in Plant Science* 16: 1649112. © Authors 2025
The figures and table are modified from Takaragawa et al. (2025).

Genetic distinctiveness of Japanese native *Saccharum spontaneum* and its importance as a genetic resource for sugarcane improvement

Sugarcane (*Saccharum* L.) is a globally important crop used not only for sugar production but also for bioenergy production to realize a low-carbon society. However, sugarcane production is increasingly threatened by climate change, which is expected to cause greater instability in yields and productivity. To address this issue, further improvement of sugarcane is required; however, breeding has been constrained by the limited genetic diversity of existing cultivars and breeding materials. To overcome these challenges, it is essential to expand genetic diversity and introduce valuable traits by effectively utilizing untapped wild genetic resources.

Saccharum spontaneum is widely distributed across tropical and subtropical regions of Asia, including both continental and island areas, and possesses a wide range of useful traits such as stress tolerance and excellent ratooning ability. Modern sugarcane cultivars have been developed through interspecific hybridization between *S. officinarum* and *S. spontaneum*. However, despite the recognized importance of *S. spontaneum*, there has been limited information on the specific contributions of its germplasm to the genetic background of modern cultivars.

In this study, we analyzed the genetic diversity of a total of 390 sugarcane genetic resources collected from all over the world. These included 135 *S. spontaneum* (including four Japanese native accessions), as well as *S. robustum* (45 accessions), *S. barberi* (15 accessions), *S. sinense* (6 accessions), and *S. maximum* (8 accessions), along with 96 modern cultivars (including seven Japanese cultivars).

The analysis revealed that *S. spontaneum* can be classified into three groups based on geographic distribution: Continental Asia Type (e.g., India and Thailand), Southeast Asia Type (e.g., Indonesia and Oceania), and Northeast Asia Type (e.g., Japan, China, and Taiwan) (Figs. 1 and 2). Furthermore, the *S. spontaneum* genomes of the Continental and Southeast Asia Types have made substantial contributions to the genetic background of modern sugarcane cultivars worldwide. In contrast, the contribution of the Northeast Asia Type was extremely limited and detected only in a small number of modern cultivars from Japan and China (Fig. 3). These findings indicate that *S. spontaneum* from Northeast Asia, particularly Japanese native accessions and Japanese cultivars with the genome, has significant importance and potential for expanding genetic diversity and introducing novel traits in future sugarcane breeding.

Authors: Terajima, Y. [JIRCAS],
Garsmeur, O., Rio, S., Pompidor, N. Hervouet, C., Durand, T.,
Hoarau, J.Y. , D'Hont, A. [CIRAD, France], and 14 others

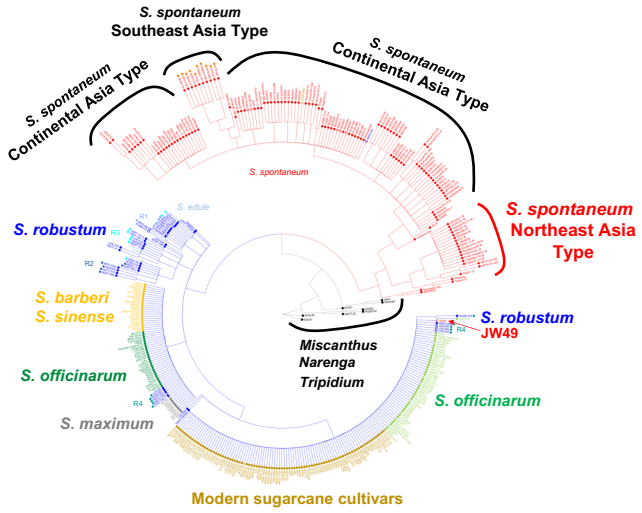

Fig. 1. Molecular phylogenetic tree of sugarcane genetic resources worldwide based on mitochondrial genome sequences

The mitochondrial genomes were assembled into single circular sequences using GetOrganelle, and phylogenetic inference was performed using MrBayes.

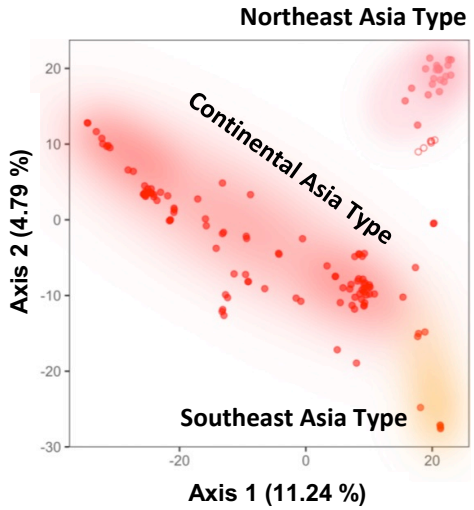

Fig. 2. Principal coordinate analysis (PCoA) of *S. spontaneum* based on single-nucleotide polymorphism (SNP) data from nuclear genomes

PCoA is an analytical method used to visualize distances among data points; greater distances between plots indicate greater genetic divergence. Axis 1 explains the largest proportion of variation among lineages, while Axis 2, which is orthogonal to Axis 1, explains the next largest proportion. The values in parentheses indicate the proportion of variance explained.

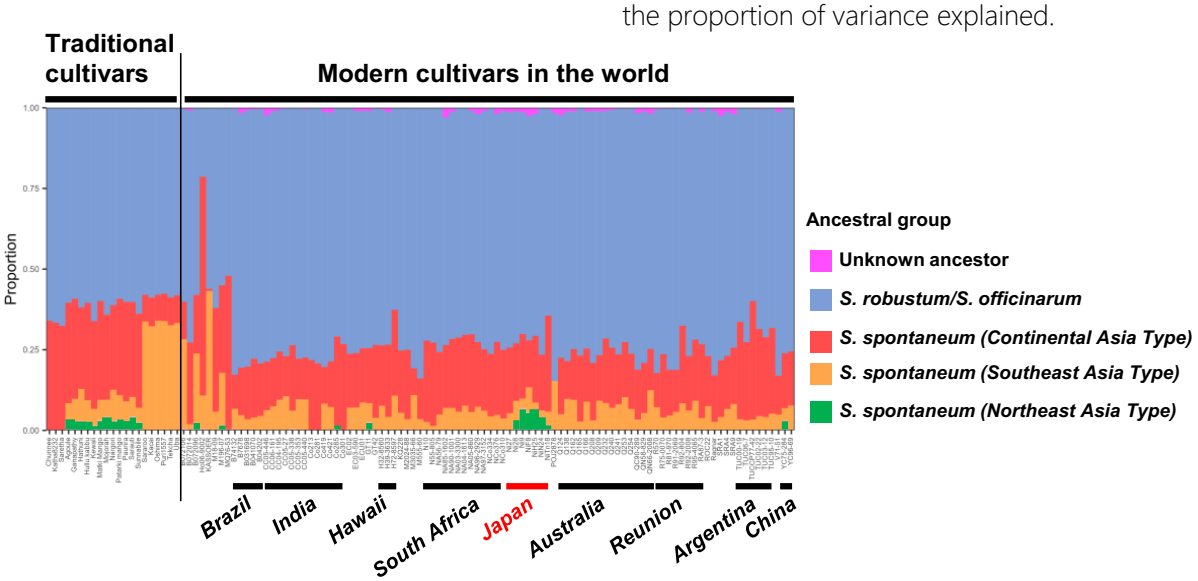

Fig. 3. Proportions of ancestral species genomes in modern and traditional sugarcane cultivars

The genomic proportions of each ancestral group were estimated by population structure analysis using species-specific DNA fragments. "Unknown ancestor" indicates previously unidentified ancestral species. Traditional cultivars classified as *S. barberi* and *S. sinense* were cultivated prior to the development of modern cultivars.

Reference: Garsmeur et al. (2025) *Cell* 188: 7252–7266.e15. © Authors 2025
The figures are reprinted/modified from Garsmeur et al. (2025) under the terms of the CC BY 4.0 license.
https://creativecommons.org/licenses/by/4.0/deed.en

A new method to breed fertile interspecific hybrids between Asian and African rice species through manipulation of ploidy level

There are two cultivated rice species in the world: Asian rice (*Oryza sativa*) and African rice (*O. glaberrima*). Nearly all rice cultivated worldwide belongs to Asian rice. African rice, the other cultivated species, was independently domesticated in West Africa and exhibits valuable traits such as resistance to diseases, tolerance to environmental stresses, and competitiveness against weeds. These traits have attracted attention as genetic resources for breeding, particularly in regions facing climate change and the need for low-input agriculture. However, F_1 hybrids between Asian and African rice show severe pollen sterility, preventing seed production. To overcome this barrier, conventional approaches have relied on backcrossing to partially introgress African rice genes into Asian rice backgrounds. As a result, the proportion of the African rice genome in such lines is typically limited. In this study, we attempted to overcome hybrid sterility by manipulating ploidy in interspecific hybrids between Asian and African rice.

First, tetraploid lines of Asian and African rice were generated through colchicine treatment. Tetraploid interspecific F_1 hybrids were then produced by crossing these lines. By culturing microspores from these tetraploid hybrids, we obtained diploid interspecific hybrids with partially restored pollen fertility. Furthermore, by culturing microspores from these diploid hybrids, doubled haploid (DH) lines were generated (Fig. 1). These plants showed high fertility, with pollen fertility reaching up to 88.4% and seed fertility up to 89.8%, comparable to the parental lines (Fig. 1). Although the proportion of Asian- and African-type alleles varied among the doubled haploid lines, two lines (DH#124 and DH#201) exhibited nearly balanced genomic contributions from both species, representing balanced genetic compositions (Fig. 1). These results demonstrate that the combination of tetraploidization to alleviate hybrid sterility and subsequent diploid induction enables the production of fertile interspecific hybrids with balanced genomic compositions between Asian and African rice, which have been difficult to obtain using conventional approaches (Fig. 2).

The interspecific hybrids developed using this method retain a higher proportion of the African rice genome compared with conventional hybrids developed through backcrossing (e.g., NERICA lines). Therefore, they may carry complex traits derived from African rice. Future work will involve detailed evaluation of agronomic traits in these hybrid materials and identification of genes underlying useful traits. This approach is expected to contribute to the development of new Asian rice varieties with improved performance under low-input conditions, including enhanced weed competitiveness and adaptation to low-fertility soils.

Authors: Kuniyoshi, D. [JIRCAS] and Kishima, Y. [Hokkaido Univ.]

Plant materials	PL9 (OS)	WK21 (OG)	DH #81	DH #84	DH #94	DH #98	DH #115	DH #124	DH #129	DH #130	DH #133	DH #201
sativa allele ratio*	1.00	0.00	0.74	0.64	0.80	0.62	0.62	0.48	0.66	0.64	0.71	0.50
Pollen fertility (%)	96.9	91.4	92.8	77.3	83.3	54.8	88.4	74.7	81.5	83.7	72.6	77.2
Seed set rate (%)	88.4	90.6	70.7	55.3	76.6	11.6	89.8	55.9	62.3	85.6	83.8	32.7

* Ratio of the *sativa* (PL9) allele within the genome of the interspecific hybrid plants (DH plants).

Fig. 1. Genomic composition and fertility of diploid doubled haploid lines

PL9 represents the *Oryza sativa* (OS) parental line, and WK21 represents the *O. glaberrima* (OG) parental line. The DH series indicates the diploid doubled haploid lines developed in this study (selected from a total of 22 individuals). These DH lines inherit genetic components from both species and exhibit both pollen and seed fertility.

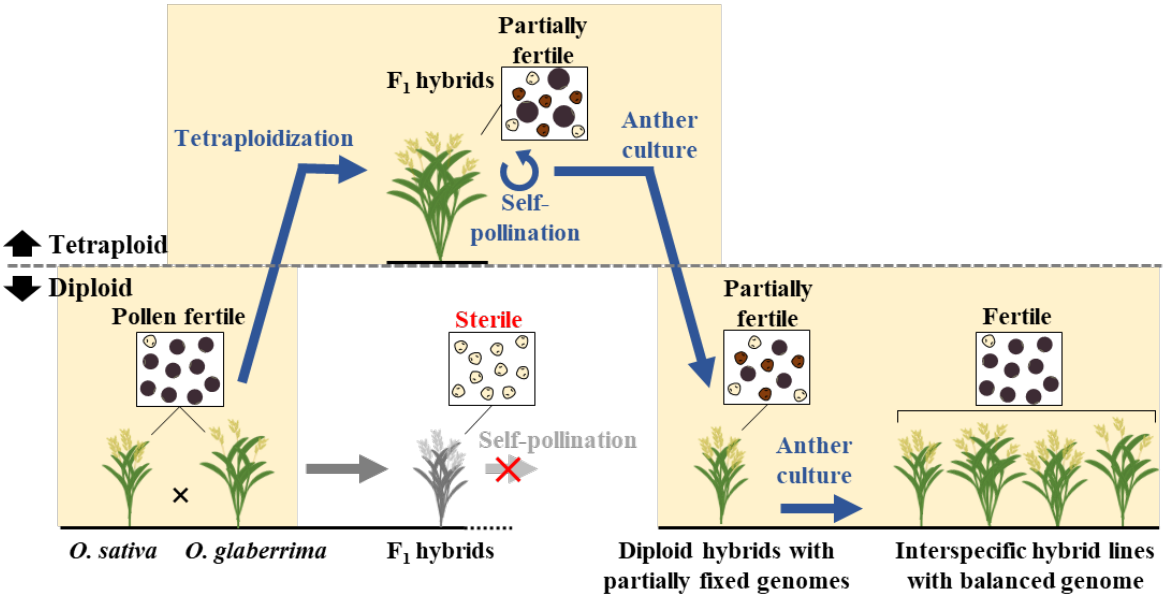

Fig. 2. Process for developing fertile hybrids by ploidy manipulation

Diploid F_1 hybrids between the two species are typically pollen sterile and cannot produce subsequent generations. However, tetraploidization temporarily alleviates pollen sterility. By culturing pollen from tetraploid plants and subsequently restoring diploidy, diploid hybrids with recovered pollen fertility and seed set can be obtained.

Reference: Kuniyoshi and Kishima (2025) *Theoretical and Applied Genetics* 138: Article 161 © Authors 2025
The figures are reprinted/modified from Kuniyoshi and Kishima (2025) under the terms of the CC BY 4.0 license.
https://creativecommons.org/licenses/by/4.0/deed.en

Japan International Research Center for Agricultural Sciences

Headquarters (Tsukuba)
1-1 Ohwashi, Tsukuba, Ibaraki
305-8686, JAPAN
TEL : +81-29-838-6313
FAX : +81-29-838-6316

Tropical Agriculture Research Front (TARF)
1091-1 Maezato-Kawarabaru, Ishigaki
Okinawa, 907-0002, JAPAN
TEL : +81-980-82-2306
FAX : +81-980-82-0614

https://www.jircas.go.jp/